

# HYDROGEN MASERS. I: THEORY AND PROSPECTS

Vladimir S. Strel'nitski <sup>1,2</sup>, Victor O. Ponomarev <sup>3</sup>, and Howard A. Smith <sup>1</sup>

<sup>1</sup> Laboratory for Astrophysics, National Air and Space Museum, Smithsonian Institution, Washington, DC 20560

<sup>2</sup> New Mexico Institute of Mining and Technology, Socorro, NM 87801

<sup>3</sup> P.N. Lebedev Physical Institute, 117924 Moscow, Leninsky prospect 53, Russia

Submitted to the *Astrophysical Journal*, Part 1

## ABSTRACT

The discovery of the first naturally occurring high gain hydrogen recombination line (HRL) maser, in the millimeter and submillimeter spectrum of the emission line star MWC349, requires an expansion of current paradigms about HRLs. In this paper we re-examine in general the physics of non-LTE populations in recombining hydrogen and specify the conditions necessary for high-gain masing and lasing in HRLs. To do so we use the extensive new results on hydrogen level populations produced by Storey and Hummer (1995), and our calculations for the net (that is, line plus continuum) absorption coefficient for the hydrogen, and we present results for the  $\alpha$ - and  $\beta$ -lines whose principal quantum numbers  $n$  are between 5 and 100, for gas whose electron number density  $3 \leq \log N_e \text{ (cm}^{-3}\text{)} \leq 11$ , at two electron temperatures,  $T_e = 5,000$  and  $10,000$  K. We show that the unsaturated maser gain in an HRL is a sharp function of  $N_e$ , and thus to achieve high-gain masing each line requires a sufficiently extended region over which the density is rather closely specified.

Saturation of masing recombination lines is a critical consideration. We derive a simple equation for estimating the degree of saturation from the observed flux density and the interferometric and/or model information about the amplification path length, avoiding the vague issue of the solid angle of masing. We also present a qualitative way to approach the effects of saturation on adjacent emission lines, although the detailed modeling is highly case-specific.

We draw attention to another non-LTE phenomenon active in hydrogen: the *overcooling* of populations. This occurs for HRLs with  $n \gtrsim 20$ , in gas where  $N_e \lesssim 10^5 \text{ cm}^{-3}$ . Observationally the HRL overcooling might manifest itself as an anomalously weak emission recombination line, or as a “dasar,” that is, an anomalously strong absorption line. In the simplest case of a homogeneous HII region the absorption can be observed on the proper free-free continuum of the region, if some conditions for the line or/and continuum optical depths are satisfied.

We briefly discuss the prospects of detecting hydrogen masers, lasers and dasars in several classes of galactic and extragalactic objects, including compact HII regions, Be or Wolf-Rayet stars, and AGNs.

*Subject headings:* masers — hydrogen: recombination lines — stars: WR stars — stars: Be stars — galaxies: AGN — stars: particular: MWC 349.

## 1. INTRODUCTION

Masing spectral lines are an efficient observational probe in astrophysics: because of their strength and narrowness they often provide the best opportunity for detailed studies of kinematics and structure of the emitting source. Until recently only *molecular* astrophysical masers have been known. Yet calculations of the atomic hydrogen level populations in HII regions which have been done since the 1930's in order to interpret optical hydrogen recombination lines (HRLs), showed that *global population inversions* probably exist across the Rydberg levels, thus raising in principle the possibility of lasing and masing in the HRLs. Numerical results directly implying inversion are found in papers like Cillié (1936), Baker and Menzel (1938), and, later, in Seaton's series of papers starting in 1959.

In spite of that, and also in spite of the fact that Menzel (1937) pointed out (even before the discovery of laboratory masers and lasers) that under non-LTE conditions the integral of energy absorbed by a line may in principle become negative, the possibility of lasing in the HRLs attracted no attention for many years. It was perhaps due partly to the deeply rooted presumptions that the correction factor for stimulated emission,  $1 - \exp(-h\nu/kT)$ , is negligible for optical lines because of their high frequency, and that HII regions are always optically thin except perhaps in the Lyman HRLs, so that no serious amplification effects are possible anyway. Only relatively recently did these assumptions change. After modeling of optical HRLs in extragalactic objects suggested HII regions of unusually high densities (up to  $N_e \sim 10^{10} \text{ cm}^{-3}$ ) and/or large extensions, Krolik and McKee (1978) considered the theoretical possibility of lasing in HRLs. Smith *et al.* (1979), analyzing their observations of an unusually intense infrared HRL in a dense HII region around the young stellar object BN in Orion, proposed that if the inversions persisted to the high densities expected in the source they could lead to laser amplification of this line.

In the mid-1960's radio recombination lines were discovered. For them the correction factor for stimulated emission is much more important than for the optical and IR lines. Goldberg (1966) showed that even in HII regions having optical thickness  $|\tau| < 1$  in both a radio recombination line and the adjacent free-free continuum, the inversion of populations can increase the line-to-continuum intensity ratio by as much as a factor of a few.

The first *high gain* HRL maser was discovered in the millimeter recombination lines in the emission line star MWC349 (Martin-Pintado *et al.* 1989a). At first the maser emission was ascribed to the ionized outflow from the star (Martin-Pintado *et al.* 1989a,b), but later it was partly (Ponomarev *et al.* 1989), and then fully, attributed to the *circumstellar disk* (Gordon 1992; Planesas *et al.* 1992; Thum *et al.* 1992). Subsequent observational and interpretational papers enlarged on the list of observed masing lines in this source, and elaborated on the model in terms of a partly ionized masing Keplerian disk [Martin-Pintado *et al.* 1989b; Thum *et al.* 1994a,b; 1995; Gordon 1994; Ponomarev *et al.* 1994 ("Paper 1"); Strelitski *et al.* 1995a; 1995b ("Paper 3")].

With the discovery of real, high gain, HRL masers in MWC349, many basic theoretical questions arise about the physics of the pumping mechanism that maintains the inversion, the dependence of maser gain on the physical parameters (density, temperature, gas velocity) of the recombining gas, and about other possible non-LTE phenomena in HRLs. Directly related to these is the more practical question of discovering these non-LTE phenomena in other lines and in other sources. Though briefly touched upon in some papers (e.g.: Walmsley 1990, Ponomarev *et al.* 1991), these questions deserve to be studied on a more systematic basis.

In this paper we readdress the theory of non-LTE phenomena in HRLs. Using the nomenclature for the non-LTE states of a quantum transition originally proposed by one of us (Strelitski, 1983), along with the recent and extensive calculations of hydrogen level populations by Storey and Hummer (1995), we analyze this phenomena (Section 2). We demonstrate that the population calculations predict not only inversion and its weaker complement, "overheating", both of which increase the intensities of emission lines, but also their opposite — "overcooling" of populations — which tends to produce an anomalously strong absorption in the line (the "dasar" effect). We briefly discuss from a physical and thermodynamical point of view how these non-LTE states are created in recombining hydrogen.

We address in Section 3 the conditions necessary for producing high maser gain in an HRL, and the conditions (and observational criteria) of *saturation*. The "net" absorption coefficient which accounts for both the negative absorption (amplification) in the line and the positive free-free absorption at the line frequencies, proved to be a useful parameter (Ponomarev 1994). Our calculations of the net absorption coefficient allow us to derive the optimum electron density  $N_e$  for strong unsaturated masing in  $\alpha$ - and

$\beta$ -lines with  $5 \leq n \leq 100$  for gas with densities up to  $N_e = 10^{12} \text{ cm}^{-3}$ , and at two representative values of electron temperature,  $T_e = 5,000$  and  $10,000$  K. The results are illustrated graphically and tabulated. Rough analytical approximations are provided for the lower  $n$  transitions. We derive a formula for estimating the degree of saturation in an observed masing HRL, if the line is formed at its optimum electron density.

Section 4 is devoted to the phenomenon of overcooling and “dasing” in HRLs. We use the solution of the line-plus-continuum radiative transfer equation for a homogenous slab to show that direct evidence of overcooling of a line would be its appearance in absorption on the free-free continuum of the HII region. We derive the minimal optical depths in the line and/or the continuum necessary for this to happen. This is not, however, the only way to detect overcooling: the increment of HRLs seen in emission can demonstrate it as well.

Finally, in Section 5, we discuss the prospects of detecting HRL masers, lasers and/or dasers in galactic and extragalactic sources other than MWC349. MWC349 itself — the only high-gain HRL maser detected so far — is addressed separately in a forthcoming paper (Strelitski *et al.* 1995b, “Paper 3”).

## 2. NON-EQUILIBRIUM STATES OF RYDBERG TRANSITIONS IN ATOMIC HYDROGEN

### 2.1. Radiative Transfer

Our analysis of non-equilibrium effects in HRLs is based on the standard solution of the radiative transfer equation for the simplest case of a steady-state, homogeneous, plane-parallel medium of finite optical thickness  $\tau_\nu$ :

$$I_\nu = S_\nu [1 - \exp(-\tau_\nu)] . \quad (2.1.1)$$

Here  $I_\nu$  is the outgoing radiation intensity at the frequency  $\nu$  and  $S_\nu$  is the source function. No external background source is assumed. In the case of the HRLs, where both line and free-free continuum are formed together, it is convenient to represent the source function as  $S_\nu = \eta_\nu B_\nu(T_e)$  (Goldberg 1966), where

$$\eta_\nu \equiv \frac{S_\nu}{B_\nu(T_e)} = \frac{k'_c + k'_l b_2}{k'_c + k'_l b_1 \beta_{12}} ; \quad (2.1.2)$$

$B_\nu(T_e)$  is the Planck function for the electron temperature  $T_e$ ;  $k'_c$  and  $k'_l$  are the continuum and the line absorption coefficients at LTE, both corrected for stimulated emission (the prime indicates LTE values);  $b_n$  is the Menzel’s coefficient of departure of the level  $n$  population from its LTE value.  $\beta_{12}$  in Eq. (2.1.2) is formally the ratio of the actual (non-LTE) and the LTE correction factors for stimulated emission (Brocklehurst and Seaton 1972):

$$\beta_{12} = \frac{1 - (b_2/b_1) \exp(-h\nu_0/kT_e)}{1 - \exp(-h\nu_0/kT_e)} , \quad (2.1.3)$$

where  $\nu_0$  is the rest frequency of the 1-2 transition and constants have their usual meanings.  $\beta_{12}$  is a measure of the deviation of the population *ratio* of two levels from its LTE value.

The net optical depth at the line center for a homogeneous medium is (we omit the subindex  $\nu_0$ ):

$$\tau_{net} = \tau_c + \tau_l = k'_c L + k'_l b_1 \beta_{12} L \equiv (k'_c + k'_l) L \equiv k_{net} L . \quad (2.1.4)$$

where  $k_l \equiv k'_l b_1 \beta_{12}$  is the actual (non-equilibrium) line absorption coefficient and  $k_{net}$  is the “net” (continuum plus line) absorption coefficient.

Since

$$I_c(\nu) = B_\nu(T_e) [1 - \exp(-\tau_c)] , \quad (2.1.5)$$

the relative line intensity at the line center is given by:

$$r(\nu_0) \equiv \frac{I(\nu_0) - I_c(\nu_0)}{I_c(\nu_0)} = \eta \frac{1 - \exp(-\tau_{net})}{1 - \exp(-\tau_c)} - 1 = \eta \frac{1 - \exp(-\tau_c - \tau_l)}{1 - \exp(-\tau_c)} - 1 . \quad (2.1.6)$$

All  $\tau$ 's and  $\eta$  here and following are at the central line frequency  $\nu_0$ , with the subindex omitted.

## 2.2. Non-Equilibrium States of a Quantum Transition

There is another commonly used parameter, besides  $\beta_{12}$ , to describe deviations of a quantum transition from equilibrium: the excitation temperature  $T_x$ , which is defined by the Boltzmann-like formula for the population ratio of the two levels:

$$\frac{N_2/g_2}{N_1/g_1} \equiv \frac{n_2}{n_1} = \exp(-h\nu_0/kT_x), \quad (2.2.1)$$

or

$$T_x = \frac{h\nu_0/k}{\ln(n_1/n_2)}. \quad (2.2.2)$$

In this subsection and in Fig. 1 we denote by  $n_i$  the population density per one degeneracy sublevel:  $n_i \equiv N_i/g_i$ , with  $g_i$  being the degeneracy of the level  $i$ ; this should not lead to a confusion with the *principal quantum number* for which the script  $n$  (without subindex) is used throughout the paper. Subindex 1 denotes the lower and 2 the upper level of the transition.

Since

$$\frac{n_2}{n_1} = \frac{b_2}{b_1} \frac{n'_2}{n'_1},$$

where primed symbols denote again the LTE values, we have the following relation between  $\beta_{12}$  and  $T_x$ :

$$\beta_{12} = \frac{1 - \exp(-h\nu_0/kT_x)}{1 - \exp(-h\nu_0/kT_e)}. \quad (2.2.3)$$

For low frequency transitions ( $h\nu_0/k \ll T_e$ ), and when also  $|T_x| \gtrsim T_e$ ,

$$\beta_{12} \approx \frac{T_e}{T_x}. \quad (2.2.4)$$

The behavior of  $T_x$  and  $\beta_{12}$ , as functions of  $n_1/n_2$ , is illustrated in Fig. 1 for the case of  $T_e = 10,000$  K and  $h\nu_0/k = 100$  K. When the population ratio  $n_1/n_2$  decreases from  $\infty$  (all the atoms in the lower level) to 0 (all the atoms in the higher level),  $T_x$  first increases from 0 to  $\infty$ , then undergoes a jump to  $-\infty$  at  $n_1 = n_2$ , and then increases to 0. The  $\beta_{12}$  parameter decreases monotonically from  $\beta_{12}^{max} = 1/(1 - \exp(-h\nu_0/kT_e))$  to  $-\infty$ , passing through 0 at  $n_1 = n_2$ .

The classification of the excitation states of a transition is most natural in terms of temperatures (Strelnitski 1983), see Fig. 1.  $T_x = T_e$  is obviously the state of *thermalization*, and  $\beta_{12} = 1$  in this state. When  $T_e < T_x < +\infty$ , we refer to the condition as one of *overheating* of the transition 1-2; it corresponds to  $0 < \beta_{12} < 1$ . The case  $T_x < 0$  (with  $\beta_{12}$  also being negative here) is the case of *population inversion*. Finally, when  $T_e > T_x > 0$  (corresponding to  $\beta_{12} > 1$ ), we call this condition *overcooling* of the transition 1-2. The choice of this nomenclature will become clearer as we analyze the observable effects of the corresponding non-LTE states below (see also Strelnitski 1983).

## 2.3. Non-Equilibrium Populations in Hydrogen

Storey and Hummer (1995) have recently completed a detailed set of calculations of the hydrogen level populations for levels  $n \leq 50$ , and presented the results as machine-readable files. For Menzel's Case B (the Lyman lines are infinitely optically thick, all other lines are thin), calculations were made for  $2 \leq \log N_e \leq 14$  and for  $2.7 \leq \log T_e \leq 5$ . Figs. 2–5, plotted with the use of the Storey and Hummer's data, show that recombining hydrogen may acquire *all* the types of non-LTE population distributions just described — overcooling, overheating and inversion.

Fig. 2 presents the  $b_n$  coefficients versus principal quantum number  $n$ , and as function of electron density,  $N_e$ , for  $T_e = 10^4$  K. The major qualitative features of the  $b_n$  behavior are:

(1)  $b_n$  tends to one when  $n$  tends to  $\infty$ . This thermalization of the highest  $n$  levels is due to the fact that their populations are dominated by three-body collisional recombinations and collisional ionizations, both processes involving the same Maxwellian gas with kinetic temperature  $T_e$ . Thus, a reservoir of quasi-thermalized levels is created at the highest  $n$ 's.

(2)  $b_n$  decreases toward lower  $n$ , due to the ever increasing rate of spontaneous decay which is roughly proportional to  $n^{-5}$ . There is a diffuse separation between those levels which are quasi-thermalized and those which are underpopulated and show a steep positive gradient  $db_n/dn$ . This boundary progressively shifts toward lower  $n$ 's, as  $N_e$  (and the effects of collisions) increases.

(3) At the lowest  $n$ 's the gradient  $db_n/dn$  tends to some high positive limiting value. Here populations are totally controlled by radiative processes, and the intrinsic trends of radiative probabilities across the levels determine this “radiative limit” in the slope of  $b_n(n)$  (compare this part of the  $b_n(n)$  curves with our  $b_n$  calculation for the case  $N_e = 0$ , shown in Fig. 2 with the broken line). The passage to the radiative regime, at low  $n$ , occurs because, at a given density, the rate of transitions induced by collisions with electrons decreases with decreasing  $n$  approximately as  $n^{4 \rightarrow 5}$ , whereas the rate of spontaneous radiative decay increases as  $n^{-5}$ . Thus the relative role of radiative processes, *at a given density*, increases with decreasing  $n$  very steeply, steeper than  $n^{-9}$ .

(4) At low enough densities ( $N_e \lesssim 10^5 \text{ cm}^{-3}$ ),  $db_n/dn$  *changes sign* before passing to the radiative limit. As seen from Eq. (2.1.3), this means that  $\beta_{12}$  exceeds +1, and thus the corresponding transitions are *overcooled*. To our knowledge, this important fact has never been pointed out before, although it has been implicitly present in the results of earlier  $(n, l)$  population calculations. It is clearly seen, for example, in Fig. 2 of Hummer and Storey (1992). The change of sign of  $db_n/dn$  is due to the onset of partial “unblurring” of the levels’ angular momentum  $l$ -structure populations at these values of  $n$ , a distribution which is blurred by proton collisions at higher  $n$ . We interpret it as follows. Unblurring begins when the radiative decay rate of an  $(n, l)$  sublevel becomes comparable with the collision rate with protons. Since spontaneous decay rates increase with decreasing  $l$ , the low  $l$  sublevels of a given  $n$  level are unblurred the first. At any given density, therefore, there is a transitional group of levels in which more and more  $l$ -sublevels (beginning with the smaller  $l$  values) are unblurred as one looks to smaller  $n$ . Blurring of the  $l$ -sublevels enables high  $l$  atoms on a level  $n$  to decay faster, via lower  $l$  sublevels, than the  $\Delta l = \pm 1$  selection rule normally allows. The more a level is unblurred the higher is the  $l$  which loses this ability to decay more rapidly. As a result, the lower the principal quantum number  $n$  the more its  $b_{nl}$  factors reflect higher populations in its higher  $l$  sublevels. This effect is seen in Fig. 3, plotted with the numerical data of Storey and Hummer (1995) for  $T_e = 10,000 \text{ K}$  and  $N_e = 10^3 \text{ cm}^{-3}$ . The effective  $b_n$  factor for a level  $n$  is derived from the statistically weighted, calculated  $b_{nl}$  factors:

$$b_n = \sum_l \frac{(2l+1)}{n^2} b_{nl}. \quad (2.3.1)$$

Since high  $l$  sublevels have higher statistical weights  $(2l+1)$ , the increase of their  $b_{nl}$  factors is more significant for the weighted value of  $b_n$  (2.3.1) than the decrease of the  $b_{nl}$  factors of low  $l$  sublevels. As a result, *unblurring increases the effective  $b_n$  value of the whole  $n$ -level*. And because the degree of unblurring increases with decreasing  $n$ , a *negative* gradient  $db_n/dn$  may result for the partly unblurred group of levels, as is seen in Fig. 2. We note that those previous calculations which neglected the angular momentum state population distributions (e.g. Walmsley 1990) show no evidence for “overcooling.”

These four features of the  $b_n$  behavior determine the shape of the  $\beta_{n,n+1}$  vs.  $n$  curves for  $\alpha$ -lines, shown in Figs. 4a,b for several values of  $N_e$ , and the shape of the  $\beta_{n,n+1}$  vs.  $N_e$  curves shown in Fig. 5 for several  $\alpha$ -transitions. Comparing Figs. 4a,b with Fig. 2 is instructive.

(1) At the high values of  $n$  the positive slope of  $b_n$  vs.  $n$  results in an *inversion* of populations —  $\beta_{n,n+1} < 0$ .

(2) In a transitional set of  $n$  values  $b_n$  levels off and then changes slope due to the unblurring of  $l$  states at progressively smaller  $n$  values; here the inversion first diminishes, and then disappears. If the density is low enough ( $N_e \lesssim 10^5 \text{ cm}^{-3}$ ), the unblurring of  $l$  states first reduces the inversion to overheating ( $0 < \beta_{n,n+1} < 1$ ), then leads to thermalization ( $\beta_{n,n+1} = 1$ ), and finally — to overcooling ( $\beta_{n,n+1} > 1$ ).

(3) The final transition of  $b_n$  to the “radiative limit,” at still lower  $n$ , stops the trend towards overcooling and brings  $\beta_{n,n+1}$  down to the slightly overheated values typical for the “radiative limit” at low  $n$ .

At low densities, therefore, the  $\beta_{n,n+1}(n)$  vs.  $n$  function has two extrema — a minimum due to inversion at high values of  $n$ , and a maximum due to overcooling at lower  $n$ 's. At densities  $N_e \gtrsim 10^5 \text{ cm}^{-3}$  there is only the inversion minimum because ion collisions at these high densities blur the  $l$ -structure down to very low  $n$ 's, and thereby remove the effective cause of overcooling.

Fig. 5 illustrates the behavior of the  $\beta_{n,n+1}$  factor as a function of  $N_e$  for some selected  $\alpha$ -transitions. Qualitatively, the  $\beta(N_e)$  functions are similar to the  $\beta(n)$  functions: high  $n$  lines (higher than  $n \approx 20$ ) have two extrema — a minimum due to inversion at high densities and a maximum due to overcooling at low densities. Lower  $n$  lines show only inversion, and this at increasingly higher densities (and diminishing amplitude) for lines of decreasing  $n$ .

#### 2.4. Thermodynamic Considerations

The creation of stable conditions for inversion, overheating, or overcooling requires cycles of population transfer which, from the thermodynamic point of view, operate as “heat pumps” (Strel'nitski 1983). The system of population transfer cycles in hydrogen is rather complicated but we can infer some general principles. The two ultimate high temperature and low temperature reservoirs that interact with the system of hydrogen levels and provide free energy to create and maintain non-equilibrium populations are, respectively, the “hot” ionizing UV radiation field and the “cold” radiation field at the lower frequency recombination lines. Note that this difference in the high-frequency and the low-frequency radiation temperatures arises not because the central star is hot: a diluted Planck spectrum with *any* color temperature possesses this gradient of radiative temperatures (Strel'nitski 1983, Sobolev *et al.* 1985). In such a radiation field the net cycle of quantum transitions is always direct (distributive) — high energy photons are split up to lower energy photons — this constitutes the content of the Rosseland theorem (Rosseland 1926; see also Strel'nitski 1983, and Sobolev *et al.* 1985). This cycle of fluorescence makes up the grand radiative-radiative (RR) pumping cycle in the recombining hydrogen in HII regions, and tends to produce a global population inversion due to the steep increase of the sink (spontaneous decay) rate with the decreasing  $n$ . However, besides the ultimate source and sink radiative reservoirs, there are other, intermediate, reservoirs involved with the process: the recombination transition levels themselves, with their excitation temperatures, and the Maxwellized gases of electrons and protons with their kinetic temperatures  $T_e$ . The heat exchange between these reservoirs provides secondary cycles of population transfer. Each of the two collisional reservoirs, free electrons and protons, have different degrees of effectiveness in their interaction with the different hydrogen levels and sublevels, and because of this difference they modify the pattern of the primary (RR) cycles and can even change, locally, the *sign* of the cycles, producing overcooling.

We note that only *one* net link — the source link or the sink link — can be collisional in these secondary cycles; the other link must be radiative. In other words: pumping cycles in hydrogen can be of the radiative-radiative (RR), collisional-radiative (CR), or radiative-collisional (RC) type, but they can not be of the collisional-collisional (CC) type because only *one* temperature,  $T_e$ , is associated with collisions in HII regions.

### 3. HYDROGEN MASERS

#### 3.1. Maser Gain

The overheating and inversion of populations occur when  $\beta_{12}$  is smaller than its LTE value  $\beta'_{12} = 1$ . It is seen from Eqs. (2.1.2), (2.1.4) and (2.1.6) that  $\eta$  is then higher than its LTE value  $\eta' = 1$ ,  $\tau_{net}$  is lower than its LTE value, and in either case it increases the relative intensity of the line. Goldberg (1966) demonstrated that in this situation the relative intensity of the line  $r$  can increase up to a factor of a few even when  $|\tau_l|$  and  $\tau_c$  are  $< 1$ .

However, to produce a maser amplification  $\gg 1$ , population inversion  $\beta_{12} < 0$  alone is not sufficient. The *net* optical depth  $\tau_{net}$  must also be negative and its absolute value must be considerably higher than unity. When  $\tau_{net} < 0$ , both  $\eta$  and the numerator in Eq. (2.1.6) are negative, and Eq. (2.1.6) becomes:

$$r \approx \frac{|\eta|}{1 - \exp(-\tau_c)} \exp |\tau_{net}|. \quad (3.1.1)$$

Thus the relative intensity of a recombination line may become very high if the exponent  $|\tau_{net}|$  (the “gain” of the maser) is  $\gg 1$ .

The maser gain is determined by the length of the amplification path,  $L$ , and the value of  $k_{net} = k'_c + k'_l b_1 \beta_{12}$  [see Eq. (2.1.4)]. A negative value of  $k_{net}$  can only derive from a negative  $\beta_{12}$ , because all the other quantities determining it are essentially positive. Since  $k'_c$ , in particular, is positive, free-free absorption always reduces the maser gain, with the amount of reduction depending on the frequency.

If the density of an HII region is not very high (say,  $\lesssim 10^8 \text{ cm}^{-3}$ ),  $\beta_{12}$  for a given transition can attain high negative values at the bottom of its inversion minimum (cf. Fig. 5), thereby increasing significantly the absolute value of  $k_l = k'_l b_1 \beta_{12}$  as compared with its LTE value  $k'_l$ . Yet, the density at which maser gain in a transition attains its maximum does *not* coincide with the density of this maximum inversion. The reason is that both  $\beta_{12}$  and  $k'_l$  depend, and depend differently, on electron density  $N_e$ , in particular with the latter having a quadratic dependence on  $N_e$ . Multiplication of  $\beta_{12}(N_e)$  by the steep ( $\propto N_e^2$ ) function  $k'_l(N_e)$  shifts the maximum of the product toward higher  $N_e$ . It also makes the range of densities with high  $|k_l|$  values much narrower than the range of densities with high  $|\beta_{12}|$  values. Furthermore, since  $k_l$  and  $k'_c$  depend on  $N_e$  differently, accounting for free-free absorption shifts (downward) somewhat the value of the density where  $k_{net}$  is minimum with respect to that for  $k_l$  alone.

In order to derive the optimum conditions for high-gain HRL masing we have performed extensive calculations of the  $k_{net}(N_e)$  dependence for  $\alpha$ - and  $\beta$ -lines with  $5 \leq n \leq 100$ . Since the minimum value of  $k_{net}$  for any line occurs at a density much higher than the density of unblurring the  $l$ -structure, our program calculating  $b_n$  coefficients neglects the  $l$ -structure as unimportant.

Several illustrative cases of the calculated  $k_{net}(N_e)$  dependence, for  $T_e = 10,000 \text{ K}$ , are shown in Figs. 6a–f ( $\alpha$ -lines) and 6g ( $\beta$ -lines). In Fig. 7 the  $k_{net}(N_e)$  dependence is given for a large interval of higher  $n$ . A logarithmic scale on the ordinate has been used to show all these lines on one graph. Only the locus of the maximal  $|k_{net}|$  values for individual lines and the *envelope* of the  $|k_{net}|(N_e)$  plots are shown for  $T_e = 5,000 \text{ K}$ . The  $k_{net}(n)$  dependence for different densities, from  $N_e = 10^3$  to  $10^{11} \text{ cm}^{-3}$ , and for the two temperatures is presented in Fig. 8.

Comparison of the  $k_{net}(N_e)$  for the  $36\alpha$  line (Fig. 6b) with the  $\beta_{n,n+1}(N_e)$  for this line (Fig. 5; the intervals of high  $|k_l|$  and  $|k_{net}|$  are indicated by the bars) shows that whereas  $\beta_{n,n+1}$  is negative over a large density interval, with a maximum of inversion that peaks at  $N_e \sim 10^5 \text{ cm}^{-3}$ , the density interval of high  $|k_{net}|$  values for this line is much narrower, and peaks at much higher density —  $N_e \sim 10^7 \text{ cm}^{-3}$ .

Table 1 gives  $N_e^{max}$ , the electron number density at which  $|k_{net}|$  attains its maximum, and the corresponding value of  $k_{net}$ , for twenty  $\alpha$ -lines and twenty  $\beta$ -lines at  $T_e = 10,000$  and  $5,000 \text{ K}$ . The dependence  $N_e^{max}(n)$  is shown graphically in Fig. 9. For the lines with  $n \lesssim 40$  (these are of particular interest because many of them have already been observed as strong masers in MWC349), we fit the following analytical approximation for  $N_e^{max}(n)$ :

$$N_e^{max} \approx 8.0 \cdot 10^{15} n^{-5.66} \quad (T_e = 10^4 \text{ K}) , \quad (3.1.2)$$

$$N_e^{max} \approx 7.7 \cdot 10^{15} n^{-5.75} \quad (T_e = 5 \cdot 10^3 \text{ K}) . \quad (3.1.3)$$

The  $k_{net}^{max}(n)$  dependence is approximated in the same interval of  $n$  by:

$$k_{net}^{max} \approx -2.3 \cdot 10^{-3} n^{-8.0} \quad (T_e = 10^4 \text{ K}) , \quad (3.1.4)$$

$$k_{net}^{max} \approx -3.4 \cdot 10^{-2} n^{-8.5} \quad (T_e = 5 \cdot 10^3 \text{ K}) . \quad (3.1.5)$$

The difference between these approximations and more exact model calculations is under  $\approx 50\%$  for  $5 \leq n \leq 40$ . The approximation (3.1.2) is drawn in Fig. 9 as a broken line.

We point out that  $N_e^{max}$  for a given transition doesn't depend strongly on the assumed temperature. It is seen in Table 1 and in Eqs. (3.1.2) and (3.1.3) which are, in fact, almost identical. For rough estimates of  $N_e^{max}$  in the whole temperature interval  $5,000 - 10,000 \text{ K}$  their “average,”

$$N_e^{max} \approx 8 \cdot 10^{15} n^{-5.7} \quad (5 \cdot 10^3 \leq T_e \leq 10^4 \text{ K}) , \quad (3.1.6)$$

can therefore be used.

In contrast,  $k_{net}(N_e^{max})$  may vary significantly with temperature, especially at the higher  $n$  values. The temperature dependence of  $k_{net}$  is more generally seen in Figs. 7 and 8.

The narrowness of the  $k_{net}(N_e)$  peaks for individual lines demonstrated in Figure 6 implies that to reach high gain masing in any small group of recombination lines around some  $n$  an extended region at



the density close to the “optimum” one for this  $n$  is required. However, if a value of  $N_e$  is fixed, rather than a value of  $n$ , the corresponding maximum value of the gain,  $|k_{net}^{max}|(N_e)$ , is *not* that of the line attaining its maximum gain at this density: there are several lines, of smaller  $n$ , whose gain is higher; likewise, there are several lines, of higher  $n$ , whose gain is smaller. This can be seen in several graphs of Fig. 6, but especially clearly in Figs. 7 and 8: the locus of  $|k_{net}|$  values for individual  $\alpha$ -lines in Fig. 7 (the two broken lines, for two temperature values) passes *below* the locus of maximal  $|k_{net}|$  values for given densities (the envelope of the individual plots). Note that both these loci are *straight lines* in the  $\log |k_{net}| - \log N_e$  graph, displaying that corresponding dependencies are of the power-law character. Fig. 8 also shows that the lower the density, the flatter the maximum of the  $|k_{net}|(n)$  function. Thus, in contrast to the case of a *given line* where a narrow density interval is required to attain the maximum possible gain, in the case of a *given density* (if the density is low enough, say,  $\lesssim 10^7 \text{ cm}^{-3}$ ) *many* lines are allowed to mase with comparable gains.

$L_1 \equiv |k_{net}|^{-1}$  is the length corresponding to  $|\tau_{net}| = 1$ . Figures 6–8, Table 1 and Eqs. (3.1.4)–(3.1.5) thus allow us to estimate how extended the medium of a given electron density should be along the line of sight to provide a maser gain  $> 1$  in a corresponding HRL. We note, however, that all these give only an *upper limit* to a  $|k_l|$  or a  $|k_{net}|$  because the calculations were done assuming the local line width is only due to the thermal broadening, ignoring possible microturbulent broadening. If the latter is present and described by an equivalent temperature  $T_{turb}$ , the value of  $|k_l|$  decreases by a factor of  $[(T_e + T_{turb})/T_e]^{1/2}$ . The relative decrease of  $|k_{net}|$  due to any microturbulent broadening (and the corresponding increase of  $L_1$ ) is even larger than that for  $|k_l|$ , because of the contribution from  $k'_c$  as seen in Eq. (2.1.4). The value of  $L_1$  may additionally be increased by the presence of large scale motions in the source (expansion, contraction) which diminish the column densities of atoms at every radial velocity (frequency), and thereby increase the value of  $L_1$  by a factor of approximately  $\Delta V/\Delta v$ , where  $\Delta V$  is the dispersion of radial velocities due to the large scale motions and  $\Delta v$  is the local radial velocity dispersion due to the thermal motions and microturbulence.

All the data for Fig. 6, Table 1, and Eqs. (3.1.2) – (3.1.5) were obtained assuming the media are *optically thin* in all recombination lines (except for the Lyman lines which, for the Menzel’s Case B, are taken to be infinitely optically thick; we do not consider these lines here). Yet, since we deal here with high-gain masers, that is with gas which is supposed to be *optically thick* in masing lines, and since, in hydrogen, the masing and pumping lines are intermixed and have comparable values of absorption coefficients, the assumption of optical thinness in all but masing lines is internally contradictory. Qualitatively, the effect of radiation trapping is similar in the “ordinary” (non-inverted) and in the inverted transition cases: the more the radiation is trapped (the larger the modulus of the line optical depth), the more the transitions induced by the trapped photons compete with spontaneous and collision-induced transitions in controlling the populations. The results of population calculations for a multilevel system with and without account for radiative trapping may, of course, differ drastically. It is impossible in practice to account in a general way for radiation trapping, not so much because it is a mathematically complicated nonlinear problem, but rather because the pattern of optical depths is peculiar to each concrete source.

Fortunately, in the important particular case of masing in a *Keplerian disk* (the case of MWC349 and similar objects) the problem of the *pumping* radiation trapping can be finessed by supposing that the medium is optically thick in only one direction, that of the chord of maximum velocity coherence (see Fig. 1 in our Paper 1). In the directions perpendicular to the disk, and also in those directions within the disk which are far from that chord, the optical depth is smaller, and it can actually be smaller than unity, even if the chord optical depth is considerably larger than unity. Since these directions occupy, all together, much larger solid angle than the directions close to the chord, spontaneously radiated photons can escape from the medium almost freely, providing an efficient pumping for high-gain, optically thick masing into relatively small solid angle *along* the chord. There is one further fact providing confidence in this general approach: the successful modeling of the masing observed in the case of MWC349 (cf. Paper 3).

If the modulus of the optical depth along the chord of maximum amplification is large enough, the rapid increase of maser intensity creates a special kind of radiation trapping problem — maser saturation.

### 3.2. Saturation

Saturation occurs when the growing maser radiation begins to influence the populations of the transitions significantly. No general solution exists for the problem of maser saturation for the same reason why no general solution is possible for radiation trapping in a system with positive optical depth. Yet, as it will be seen below and in Paper 3, saturation may be occurring in these systems, and understanding its role will play a crucial part in interpreting the observed properties of masing HRLs, and in predicting the observability of other lines. In this section we consider two basic questions concerning saturation in HRLs: (1) how saturation in a masing line affects the level populations (thus the gain) of the masing transition itself; and (2) how, in a multi-line HRL maser, saturation in one line affects the populations and the maser gains in adjacent lines. We also derive a criterion for suspecting when saturation has occurred in a masing HRL.

The first question has been intensively studied in the context of molecular masers. The condition of saturation is that the maser radiation density influences “noticeably” the population difference  $\Delta N_{21}$  between the upper (2) and lower (1) maser levels. Ideally one needs an analytical expression for  $\Delta N_{21}$  as a function of all the basic processes influencing the populations. In practice this goal is unattainable when the number of interacting levels is  $> 3 - 4$ . Several simplifying approaches have therefore been proposed to get around this problem (see the discussion in Streltinski, 1993). In all these approaches the two *relaxation* processes, radiative (maser) and collisional transitions between the maser levels themselves, are accounted for almost exactly. It is much more difficult, however, to provide for a complex system a simple yet adequate approximation for all the *pumping* processes.

In one approach, pumping is represented by four phenomenological coefficients for the upper and lower maser levels: the “income” coefficients  $\lambda_2$  and  $\lambda_1$  ( $\text{cm}^{-3} \text{s}^{-1}$ ) and the “outlay” coefficients  $\Gamma_2$  and  $\Gamma_1$  ( $\text{s}^{-1}$ ). Omitting subindex “12” where it cannot lead to misunderstanding, and taking for simplicity the degeneracies of the maser levels to be equal, the solution of the statistical equilibrium equations in this “ $\lambda, \Gamma$ ”-approach can be represented as follows (e.g.: Streltinski, 1993):

$$\Delta N = \frac{\Delta N_0}{1 + \frac{BJ}{\Gamma + C_{21}}} = \frac{\Delta N_0}{1 + \frac{J}{J_s}}, \quad (3.2.1)$$

where

$$\Delta N_0 = \frac{\frac{\lambda_2}{1 + \Gamma_2/\Gamma_1} - \frac{\lambda_1}{1 + \Gamma_1/\Gamma_2}}{\Gamma + C_{21}} \quad (3.2.2)$$

is the unsaturated population difference;  $\Gamma \equiv (\Gamma_2^{-1} + \Gamma_1^{-1})^{-1}$  is the harmonic mean value of the decay rate of the two levels;  $B$  is the Einstein coefficient for induced radiative transitions between the maser levels ( $B \equiv B_{12} = B_{21}$  since we assumed the degeneracies of the two levels to be equal);  $J$  is the actual radiation intensity averaged over the profile of the absorption coefficient and over directions;

$$J_s \equiv (\Gamma + C_{21})/B \quad (3.2.3)$$

is the so called “saturation intensity;” and  $C_{21}$  is the rate of collisional relaxation between the maser levels. To obtain this form of eqs. (3.2.1) and (3.2.2) we ignored the slight differences between  $C_{12}$  and  $C_{21}$ . Strictly speaking, then, these equations are only valid for transitions with  $h\nu \ll kT_e$  which, at  $T_e \sim 10^4 \text{ K}$ , comprise all hydrogen  $\alpha$ -lines down to  $\approx 5\alpha$ .

Eq. (3.2.1) shows that maser radiation begins to influence the maser level populations when the rate of its interaction with the maser levels,  $BJ$ , becomes comparable to the higher of the two rates: the rate of collisional relaxation between the levels,  $C_{21}$ , and the rate of the decay of the populations from the maser levels in the pumping processes,  $\Gamma$ . (It is worth noting that harmonic mean is always smaller than the smallest of the two averaged numbers, and equal to one half of each when they are equal.) The *net* effect of the maser radiation is the transfer of population from the upper to the lower state. It is seen in Eq. (3.2.1) that in the limit  $J \gg J_s$  the population difference  $\Delta N \rightarrow 0$ , and thus  $(N_2/N_1) \rightarrow 1$ . Note, however, that in this limit,  $\Delta N \propto J^{-1}$  [see Eq. (3.2.1) with  $J \gg J_s$ ]. This dependence of  $\Delta N$  on  $J$  reduces the maser amplification from an exponential [Eq. (3.1.1)] to a linear dependence. The effect is easily understood by noting that the radiative transfer equation for a sufficiently strong maser (where the spontaneous term is negligible when compared to the induced term) reduces to:

$$\frac{dI}{dz} = \frac{h\nu}{4\pi} B \Delta N I.$$

When  $\Delta N$  is independent of the intensity  $I$  (unsaturated regime), integration gives an exponential growth of  $I$  with  $z$ ; when  $\Delta N \propto I^{-1}$  (saturation),  $I$  depends on  $z$  linearly (see also general reviews of maser theory, e.g., Strel'nitski, 1974; Reid and Moran, 1981; Elitzur, 1992).

The major simplifying assumption of the “ $\lambda, \Gamma$ ”-approach is that  $\lambda_2$  and  $\lambda_1$  do not depend on the maser level populations. This leads eventually to the expression (3.2.1) which states that  $(\Delta N/\Delta N_0)$  does not depend on  $\lambda$ 's but only on  $\Gamma$ 's and  $C$  — a radical simplification. The fewer the number of the levels involved with the pumping, the worse the approximation, because in such a few-level system the non-maser level populations — the source of “income” for the maser levels — depend sensitively on the populations of the maser levels.

In the case of HRLs pumped by recombinations, cascading and collisions, every level is fed by *many* other levels. If there is only one masing transition in the system, the change of its populations caused by saturation should not produce any serious distortion of the reservoir of pumping. Moreover, even if masing and saturation occur in *several* adjacent lines in the same region of space, this will hardly change the reservoir of pumping for individual transitions because saturation only re-distributes populations between two adjacent levels, without bringing populations in or out of the reservoir as a whole. Thus the “ $\lambda, \Gamma$ ”-approximation should give an adequate qualitative description of the  $\Delta N(J)$  dependence for individual masing recombination lines, in spite of the fact that in hydrogen the reservoir of populations for pumping may heavily overlap with masing transitions.

The hydrogen levels we consider here decay primarily through spontaneous and collision-induced transitions to other levels; thus,

$$\Gamma \approx A_t + C_t, \quad (3.2.4)$$

where  $A_t \equiv (A_{t1}^{-1} + A_{t2}^{-1})^{-1}$  and  $C_t \equiv (C_{t1}^{-1} + C_{t2}^{-1})^{-1}$  are the harmonic mean values of the total Einstein  $A$  coefficient and of the total collision rate for the two maser levels respectively. Using Eq. (3.2.4) and the relation between the Einstein  $A$  and  $B$  coefficients, we can rewrite Eq. (3.2.3) as

$$J_s \approx \frac{2h\nu_0^3}{c^2} \frac{A_t + C_t + C_{21}}{A_{21}}, \quad (3.2.5)$$

where  $A_{21}$  is the Einstein coefficient for the maser transition,  $\nu_0$  is the transition frequency and the constants have their usual meanings.

To estimate the degree of saturation in an observed masing line, we have to compare an estimate of  $J$  in the source with  $J_s$  given by Eq. (3.2.5). A key and complex issue is that of the radiation's solid angle, but we are able to sidestep the matter using the following argument (cf., Strel'nitski, 1984). On the one hand, unless the geometry of the source is very special, the solid angle of the maser beam should be close to

$$\Omega \approx \frac{\sigma}{l^2}, \quad (3.2.6)$$

where  $\sigma$  is the observed emitting surface area, and  $l$  is the amplification path length. On the other hand, the solid angle under which we see the source is

$$\omega \approx \frac{\sigma}{D^2}, \quad (3.2.7)$$

where  $D$  is the distance to the source.

Thus,  $\sigma$  cancels out in the equation connecting  $J$  with the observed flux density  $S$ :

$$J = I \frac{\Omega}{4\pi} = \frac{S}{\omega} \frac{\Omega}{4\pi} = S \frac{D^2}{4\pi l^2}, \quad (3.2.8)$$

where  $I$  is the specific radiation intensity averaged over the profile of the absorption coefficient. From Eqs. (3.2.5) and (3.2.8) we obtain the degree of maser saturation:

$$\frac{J}{J_s} \approx \frac{c^2 D^2}{8\pi h\nu_0^3} \frac{A_{21}}{A_t + C_t + C_{21}} \frac{S}{l^2}. \quad (3.2.9)$$

Eq. (3.2.9) gives an estimate of the degree of saturation in terms of the transition constants  $\nu_0$ ,  $A_{21}$ ,  $A_t$ , the model parameters  $C_t$ ,  $C_{21}$  (determined by the model density of the emitting region),

the observed flux parameter  $S$ , and the “semi-observed” parameter  $l$  which, though not directly observable, can in principle be reliably estimated from direct interferometry of the source structure in the plane of the sky and the geometrical model of the source. We emphasize that transition to saturation is a *gradual* process. It is seen from Eq. (3.2.1) that to pass from an unsaturated regime ( $J/J_s \ll 1$ ) to a heavily saturated one ( $J/J_s \gg 1$ ), the intensity needs to increase by about two orders of magnitude. Thus the saturation criterion  $J > J_s$  is no more than an *order of magnitude* criterion.

There is one case for which we can simplify Eq. (3.2.9) without losing its exactness: the case where maser radiation is generated at the “optimum” density, i.e., the density that provides the maximum (unsaturated) value of  $|k_{net}|$  for the line in question. As was discussed in Section 3.1, the optimum density for maser amplification is much higher than the density of maximum inversion, and, as Figs. 5 and 6 show, this optimum density is actually rather close to the density of thermalization. At such high densities,  $A_t$  in Eq. (3.2.9) can always be ignored as compared with  $(C_t + C_{21})$ . For  $5 < n < 35$  and  $T_e = 10^4$  K, we use the following approximation:

$$\delta \equiv (C_t + C_{21}) \approx 3 \cdot 10^{-9} n^5 N_e, \quad (3.2.10)$$

which is a simplified version based on Gee’s *et al.* (1976) analytical approximations for collision rates and which is exact to  $\pm 5\%$ . Substituting for  $N_e$  the approximation (3.1.6) for  $N_e^{max}$ , and taking  $A_{21} \approx 6.3 \cdot 10^9 n_1^{-5} (\text{s}^{-1})$  and  $\nu_0 \approx 6.6 \cdot 10^{15} n_1^{-3} (\text{s}^{-1})$  — common approximations valid for  $\alpha$ -lines with  $n \gg 1$  — and finally neglecting  $A_t$  in Eq. (3.2.9) as compared with  $(C_t + C_{21})$ , the equation reduces to

$$\frac{J}{J_s} \approx 0.2 \left( \frac{D}{\text{kpc}} \right)^2 \left( \frac{n}{10} \right)^{4.7} \left( \frac{S}{\text{Jy}} \right) \left( \frac{10^{13} \text{ cm}}{l} \right)^2. \quad (3.2.11)$$

The previous assumption, that the observed masing lines arise in regions of “optimum” density, is of course an assumption which can be wrong. One reason may be the interaction of the adjacent masing transitions due to saturation. Suppose some line  $2 \rightarrow 1$  mases at its optimum density and reaches strong saturation. We can ask how such saturation might affect the trends of masing in the next transition higher,  $3 \rightarrow 2$ . If the  $2 \rightarrow 1$  line were not saturated, the  $3 \rightarrow 2$  line would be if not thermalized, at this high density, at least amplifying less strongly than its own optimum (lower) density would predict (see Fig.5 for an illustration). According to Eq. (3.2.1), however, saturation of the  $2 \rightarrow 1$  transition means that  $\Delta N_{21}$  decreases due to the transfer of some population from level 2 to level 1, and implies that the population of the lower level of the  $3 \rightarrow 2$  transition decreases. In other words, *saturation of the transition  $2 \rightarrow 1$  should increase the inversion of the transition  $3 \rightarrow 2$* . In thermodynamic language, saturation of the transition  $2 \rightarrow 1$  opens a new channel of sink to the maser on the transition  $3 \rightarrow 2$ , thereby increasing the efficiency of its pumping. As a result, the  $3 \rightarrow 2$  line will be amplified to a higher intensity. If it in turn saturates, it will increase in the same manner the inversion of the next higher transition, etc. The efficiency of this upward diffusion of the reenforced pump sink decreases, however, at every step, until eventually, at some higher value of  $n$ , the steeply increasing relative rate of thermalizing collisions will remove the population inversion.

Thus, a saturated high frequency masing line can “attract” an adjacent group of lower frequency lines to mase in a region of density higher than their unsaturated “optimum” densities. We will apply this mechanism, in Paper 3, to interpreting some observed properties of the multi-line hydrogen maser in MWC349. In any particular case, however, this qualitative idea requires a more exact numerical check — a calculation of level populations including induced radiative transitions in the lines which are supposed to be saturated masers.

#### 4. HYDROGEN “DASARS”

The effect of overcooling, demonstrated for hydrogen Rydberg levels in Fig. 4a and 5 and discussed in Section 2.3, is actually a well known phenomenon for radio lines of some interstellar molecules ( $\text{H}_2\text{CO}$ ,  $\text{OH}$ ). Observationally it appears as an enhancement of a line seen in absorption. The observational effect of overcooling was called “DASAR” (“Darkness Amplification by the Stimulated Absorption of Radiation”) by C. Townes and A. Shawlow. Overcooling is sometimes called “anti-inversion,” and the corresponding enhanced absorption — “anti-maser.” The analysis of non-LTE states of a quantum transition given in

Section 2.2 shows, however, that overcooling is really more an analogue of overheating than of inversion (see more in Streltinski, 1983).

We first show that for an homogeneous, ionized cloud with no external continuum background, the observation of a line in absorption, i.e.,  $r < 0$ , *requires*  $\beta_{12} > 1$  – overcooling of the corresponding transition.

From Eq. (2.1.6),  $r < 0$  corresponds to

$$\eta < \frac{1 - \exp(-\tau_c)}{1 - \exp(-\tau_c - \tau_l)} . \quad (4.1.1)$$

It is easily seen that the right-hand side of Eq. (4.1.1) is always  $< 1$ , whatever the value (or sign) of  $\tau_l$ , and hence  $\eta < 1$ , which is only possible according to Eq. (2.1.2) if  $\beta_{12} > 1$ .

Thus, in the framework of this simple model, the very observation of a recombination line in absorption on the proper free-free continuum of the cloud is a direct indication that the transition is overcooled. More complicated circumstances, however — a hotter external continuum background for example, or some peculiar morphology of the cloud, like perhaps if the kinetic temperature decreases radially outward — can produce an absorption recombination line without overcooling. Usually such cases can be identified by a detailed analysis of the source.

Unfortunately, the reverse statement, namely that  $\beta_{12} > 1$  (overcooling) *always* results in  $r < 0$  (a line seen in absorption), is not true. To see when overcooling does produce an absorption line in our model, we consider three particular cases:

- (1)  $\tau_c \ll 1$ ,  $\tau_l \ll 1$ ;
- (2)  $\tau_c \ll 1$ ,  $\tau_l \gtrsim 1$ ;
- (3)  $\tau_c \gtrsim 1$ .

In the first case, expanding the exponents in Eq. (2.1.6) to first order terms and using Eqs. (2.1.2) and (2.1.4), we have:

$$r \approx \eta \frac{\tau_{net}}{\tau_c} - 1 = \frac{k'_l}{k'_c} b_2 . \quad (4.1.2)$$

Since all the terms on the right-hand side are positive,  $r$  can only be positive in this case. In other words, only *emission* recombination lines can be observed from an optically thin cloud with no external continuum background.

Case (2) can occur for high frequency recombination lines ( $n \lesssim 30$ ), for which  $k'_c \ll k'_l$  (see Fig.10). Ignoring  $k'_c$  in Eq. (2.1.2) and expanding the denominator on the right-hand side of Eq. (2.1.6) to first order, we have, as the condition of  $r < 0$  for this case:

$$\tau_c > \frac{1 - \exp(-\tau_l)}{\beta_{12}} . \quad (4.1.3)$$

Thus, for high frequency lines overcooling can produce an absorption line even in a cloud optically thin in the continuum, however, the line optical depth of the cloud needs to be  $\gtrsim 1$  and its continuum optical depth should satisfy the condition above (4.1.3).

Finally, we consider case (3), first in its asymptotic form, when  $\tau_c \gg 1$ . Eq. (2.1.6) reduces then to  $r \approx \eta - 1$ , and the condition  $r < 0$  becomes  $\eta < 1$  which, according to Eq. (2.1.2), is identically satisfied if  $\beta_{12} > 1$ . Thus, for a homogeneous cloud optically thick in continuum an overcooled recombination line will always be observed in absorption (whatever the value of  $\tau_l$ ).

Now we show that this is true even for a *moderately* optically thick cloud ( $\tau_c \gtrsim 1$ ). In this case both numerator and denominator in Eq. (2.1.6) are less than 1 and greater than  $(1 - e^{-1}) \approx 0.63$ . Thus the condition  $r < 0$  in this case becomes  $\eta < 0.63$ . After some algebra on equation (2.1.2) for  $\eta$ , and remembering that  $b_2/b_1 < 1$  when  $\beta > 1$ , the  $r < 0$  condition becomes:

$$\frac{k'_l b_1}{k'_c} > \frac{0.6}{\beta_{12} - 1.6} . \quad (4.1.4)$$

Taking  $\beta_{12}$  (at its maximum) from Fig. 5,  $b_1$  from Fig. 2, and  $k'_l, k'_c$  from Fig. 10, it is easy to see that Eq. (4.1.4) is satisfied for all the transitions which can be overcooled in principle,  $n \gtrsim 20$  up to at least  $n = 56$ , seen in Fig. 5. Thus, for all these transitions (and in fact for higher  $n$  transitions as well) overcooled lines will be observed in absorption, if  $\tau_c \gtrsim 1$ .

Observation of an absorption line on the proper free-free continuum of an HII region is the most direct way to reveal overcooling, but it is not the only possible way. At low optical depths (Case 1) there is another obvious way: to observe *more than one* line in the interval of  $n$  where overcooling is theoretically predicted and to determine the decrement of  $r$  with respect to  $n$ . According to Eq. (4.1.2), in the optically thin case  $r \propto b_n$ , hence, the observed *sign* of the decrement of  $r$  should show whether or not overcooling takes place.

## 5. PROSPECTS

In this Section we address the observational prospects for HRL masers, lasers, and dasars. Our analysis of masing shows that there are at least two preliminary questions to be addressed when considering an object, or a class of objects, as a potential candidate: (1) what are the *densities* of ionized hydrogen in the source? and (2) what is the linear scale, or, more exactly, the column density per thermal line width, at each density? The answer to the first question shows us which lines might be inverted or overcooled in the source, the answer to the second — whether or not these non-LTE lines can become high gain masers or detectable dasars.

We examine now, with these two test questions, several classes of objects. This list of candidates should not be regarded as a complete one: we only give several examples. We do not discuss here the objects similar to MWC349 — hot emission line stars with neutral disks ionized on their surface. Some observational prospects regarding this class of sources will be presented in Paper 3.

### 5.1. Compact HII Regions

Simple estimates show that among the compact HII regions associated with the sites of massive star formation, only the densest, “ultracompact,” ones can have optical depths in HRL close or surpassing unity by absolute value as required for masing. Typical electron densities in ultracompact HII regions are  $N_e \sim 10^4\text{--}10^5\text{ cm}^{-3}$ , but in some of them an *average* density is estimated to be as much as  $N_e \approx 3 \cdot 10^5\text{ cm}^{-3}$  (Wood and Churchwell 1989; Kurtz *et al.* 1993). Figure 8 shows that the lines in a broad interval, from  $\approx 35\alpha$  to  $\approx 60\alpha$ , have comparably high  $|k_{net}|$  at this density, which may reach  $\sim 10^{17}\text{ cm}^{-1}$ , if the temperature is somewhat lower than 10,000 K. Since many of these ultracompact HII regions have dimensions  $L \gtrsim 10^{17}\text{ cm}$ , the maser gain  $|k_{net}|L$  may surpass unity in these lines, even if the velocity dispersion reduces the effective value of  $|k_{net}|$  by a factor of 1.5–2. Thus, some increase of intensity and line narrowing due to masing is anticipated in this interval of  $\alpha$ -lines from the most compact HII regions.

Some of these regions are highly inhomogeneous. Since chances of high-gain masing increase, in general, with the increasing density, masing in lower  $n$  lines is also quite possible from local density enhancements, even if such zones of higher density are considerably smaller than the dimensions corresponding to the average density of the object.

HII regions associated with evolved objects, for example planetary nebulae, have in general lower densities. Nevertheless studies of forbidden line transitions (e.g., Osterbrock, 1989) show that in some cases like IC4997 there are regions with densities up to  $10^6\text{ cm}^{-3}$ .

Effects of masing can be studied by comparing the intensities and widths of several  $\alpha$ -lines over a broad range of  $n$ , and also by comparison with the  $\beta$ -lines from nearby  $n$  (see Paper 3). The analysis would help specify more exactly the physical parameters of the HII region.

### 5.2. Wolf-Rayet Stars

The idea to search for HRL line masers in Wolf-Rayet (WR) stars originated with H.E. Matthews (1992; private communication). These stars possess strong winds and expanding ionized circumstellar disks which might promote population inversions and maser amplification similar to those in the disk of MWC349. However, the first attempts to find mm and submm hydrogen masers in WR stars gave negative results (Matthews 1994; private communication).

The most probable reason is insufficient optical depth in the lines ( $30\alpha$  -  $26\alpha$ ) studied. They require  $N_e \sim 10^7$ – $10^8$  cm $^{-3}$  (see Table 1) for effective masing — but these densities are not sustained in large enough *column* densities in a WR disk outflow. If we approximate the ionized envelope of a WR star as a spherically symmetric,  $\gtrsim 1000$  km s $^{-1}$  constant velocity (thus  $N_e \propto R^{-2}$ ) outflow with a mass loss rate of  $\lesssim 10^{-4} M_\odot$  yr $^{-1}$ , it is easy to show that the linear scale of the region of density  $N_e$  will be  $R(N_e) \lesssim 2 \cdot 10^{18} N_e^{-1/2}$  cm. At the optimum density of the H26 $\alpha$  line, for example, where  $N_e^{max} \approx 1 \cdot 10^8$  cm $^{-3}$ , we find  $R(N_e^{max}) \lesssim 2 \cdot 10^{14}$  cm. Table 1 gives  $k_{net}^{max} \sim -10^{-14}$  cm $^{-1}$  for this line, but, in calculating the optical thickness we must reduce this value by the ratio of the radial velocity dispersion in a WR envelope,  $\Delta V \sim 10^3$  km s $^{-1}$ , to the thermal line width,  $v_{th} \sim 20$  km s $^{-1}$  (see Sect. 3.1). As a result, the net optical depth in the line reduces to  $\tau_{net} \approx k_{net} R(N_e^{max}) (v_{th}/\Delta V) \sim -10^{-2}$ . In the same way we can show that  $|\tau_{net}| \ll 1$  for other mm and submm lines. Though  $|\tau_{net}|$  does increase with decreasing  $n$ , it becomes  $\gtrsim 1$  only at  $n \lesssim 10$ . Thus, high gain lasers in hydrogen recombination  $\alpha$ -lines from the expanding shells of WR stars are most promising for the IR lines with  $n \lesssim 10$ .

At this high a frequency a different source of line emission can be even more effective at producing laser lines in WR stars: the *atmosphere*. In the standard model of a WR star the non-expanding atmosphere consists of a turbulent layer where  $N_e \sim 10^{11}$ – $10^{13}$  cm $^{-3}$  and which is  $\sim 5 \cdot 10^{11}$  cm thick. Such densities are optimum for lasing in  $n \lesssim 7$  lines (see Table 1). Multiplying the width of this layer by our calculated values of  $k_{net}^{max}$ , we find very large optical depths; with  $N_e \sim 10^{12}$  cm $^{-3}$ , for example, the optical depth of B $\alpha$  should be  $\sim -200$ ! Even assuming the lower limit to the density in this layer (deduced by Aller from optical spectroscopy) of  $N_e \sim 10^{11}$  cm $^{-3}$ , we still have optical depths of  $-0.2$ ,  $-3$ , and  $-2$  for the B $\alpha$ , H6 $\alpha$ , and H7 $\alpha$  lines respectively, with B $\alpha$  being the most promising line if the density is higher than this lower limit.

The observability of an HRL laser is, however, strongly contingent upon its geometry. If the solid angle of lasing is not small enough, this emission tends to be lost on the stronger, spontaneous emission background. This problem is discussed in more detail in Paper 3.

### 5.3. Be Stars

Smith et al. (1979) suggested that Be stars might be likely candidates for lasing in the infrared hydrogen lines, although at that time the lack of theoretical high density population data precluded a quantitative discussion. These complex objects have ionized Keplerian disks (Slettebak *et al.* 1992), high mass loss rates, photometric variability, and, most important for our considerations, inferred densities in the region emitting Balmer lines of  $N_e \sim 10^{11}$ – $10^{13}$  cm $^{-3}$ , over dimensions  $\sim 10^{12}$ – $10^{13}$  cm. These parameters are similar to those in the turbulent layer of a WR atmosphere, and similar considerations hold here too, suggesting they are promising candidates for lasing in the near IR recombination  $\alpha$ -lines ( $n \lesssim 10$ ).

### 5.4. Active Galactic Nuclei and Starburst Galaxies

Enormous masses of ionized hydrogen are present in the central parts of galaxies with active nuclei (AGN), while starburst galaxies, which may sometimes be the result of two galaxies in collision, often have bright compact HII regions outside the nucleus. In the case of AGN's we consider the possibilities of maser action in two types of regions (e.g., Osterbrock 1989). In the so-called "Broad Line Regions" (BLR)  $N_e \sim 10^8$ – $10^{10}$  cm $^{-3}$ , and may range between  $L \sim 0.01$ – $0.1$  pc (Seifert 1 galaxies) to  $\sim 1$  pc (quasars). In the "Narrow Line Regions" (NLR)  $N_e \sim 10^2$ – $10^4$  cm $^{-3}$ ,  $L \lesssim 1000$  pc. However, the densities above do not apply to these linear scales but rather to much smaller "clumps" or cloudlets—the filling factor should be much less than one.

At the densities typical for BLR, H $\alpha$ -lines with  $n \approx 10$ – $25$  have maximum local maser gain (Fig. 8). Taking the values of  $k_{net}^{max}$  for these lines from Fig. 6 or Table 1, we see that linear scales of only  $\sim 10$  AU (25 $\alpha$ ) to  $\sim 0.01$  AU (10 $\alpha$ ) are needed to make these lines optically thick, if line broadening is thermal. If the individual cloudlets in BLR are of these dimensions or bigger, then laser emission in these submm and IR lines is anticipated, and would be seen as relatively strong narrow features centered at the radial velocities of individual cloudlets. It seems quite possible. For example, in the Scoville and Norman

(1988) model of the broad emission line clouds as photoionized mass-loss envelopes of giant stars, the Strömgren sphere reaches down to a radius of  $\sim 10^{14}$  cm in the stellar envelope. With the density there being  $\sim 10^9 \text{ cm}^{-3}$ , the  $10\alpha$ - $15\alpha$  lines should have high unsaturated laser gains — on the order of tens.

The NLR gas seems to be a less likely prospect for high-gain masing in HRLs. The densities of the NLR gas are optimum for masing in high  $n$   $\alpha$ -lines —  $n \gtrsim 50$ . Densities  $\sim 10^4 \text{ cm}^{-3}$  have linear scales up to  $\sim 1$  pc in AGNs (viz., the ionized accretion disk “halo” postulated by Scoville and Norman, 1995). According to Fig. 8, the  $50\alpha$  –  $80\alpha$  lines have the highest  $|k_{\text{net}}|$  at this density, but it is easy to see that maser gains of only  $\lesssim 0.1$  are achievable. The regions with  $N_e \sim 10^2 \text{ cm}^{-3}$  can be much larger, up to  $\sim 1$  kpc, but considering the velocity dispersion in such a large region, we have to reduce the optical depth at each frequency by a factor of  $\Delta V/v_{\text{th}} \approx 50$ , and  $\tau_{\text{net}}$  turns then out to be  $< 1$  in this case too.

Maser effects in mm HRLs are anticipated in the starburst galaxies whose archetype, M82, was in fact the first external galaxy where a radio recombination line ( $\text{H}166\alpha$ ) had been detected (Shaver *et al.* 1977). Kronberg *et al.* (1985) postulate dense ( $N_e \sim 10^7 \text{ cm}^{-3}$ ) ionized shells surrounding supernovae which had exploded inside dense molecular clouds of the M82-like starburst galaxies. According to Fig. 8,  $\alpha$ -lines with  $n \approx 20$ – $35$  have the highest maser gains at this density. With the typical linear scale for the shells being  $\sim 3 \cdot 10^{16}$  cm, Fig. 8 shows that the gain can surpass unity, if large-scale motions do not broaden the HRL too much, as compared with the thermal width, and if  $T_e$  is not much higher than 10,000 K. Though the both latter assumptions can be wrong, some indications of narrow, presumably weakly masing components in the  $36\alpha$  line from M82 has recently been detected by Smith *et al.* (1995).

#### 5.4. Hydrogen Dasars

From an observational point of view the major difficulty with the overcooling phenomenon in HRLs, as compared with inversion, is the low upper limit for  $N_e$ : overcooling disappears at  $N_e \gtrsim 10^5 \text{ cm}^{-3}$  (see Sect. 4). At this limiting density hydrogen  $\alpha$ -lines with  $n \approx 20$ – $25$  are overcooled, and the Case 2 (cf., Sect. 4) applies. Since  $\beta_{12}$  is only slightly greater than 1 for these lines, Eq. (4.1.3) shows that  $\tau_l$  must be  $> 1$  to observe an absorption line on the proper continuum of an HII region. The typical value of  $k_l$  for these lines, at  $N_e \sim 10^5 \text{ cm}^{-3}$ , is  $k_l \sim 10^{-20} \text{ cm}^{-1}$  (Fig. 10), and thus very large HII region dimensions, of  $> 300$  pc, are needed for  $\tau_l > 1$ . HII regions with such parameters are unknown.

At lower densities, which might make it easier to find larger regions, the maximum of overcooling shifts to the higher  $n$  lines. The values of  $b_n$ ,  $\beta_{12}$  and the oscillator strengths of the lines all increase, but the  $N_e^2$  factor decreases faster, so the required linear scale increases. Of known objects, we believe only AGN’s can be considered today as possible candidates for *direct* observations of hydrogen dasars. If the regions of intermediate density,  $N_e \sim 10^4 \text{ cm}^{-3}$ , have dimensions comparable with NLR’s (up to  $\sim 1000$  pc),  $\alpha$ -lines from  $n \approx 30$ – $35$  may acquire  $\tau_l \sim 1$  and appear as dasars.

The most realistic way to detect the effect of overcooling in hydrogen, however, is to observe more than one line in the  $n$  range where overcooling is predicted at a given density, and to determine the decrement of  $r$  with  $n$ , as described in Sect. 4. This way of inferring overcooling is applicable to any galactic HII region if the observations are done in the proper frequency range.

## 6. CONCLUDING REMARKS

Hydrogen, the simplest and the most abundant atom in the Universe, is also the first known *atomic* astrophysical maser. Perhaps the most striking feature of this maser, as compared with *molecular* astrophysical masers, is its obstinate uniqueness: six years after its discovery in MWC349 there is still only one known strong hydrogen maser source, despite intense attempts to find another. In contrast, practically every newly discovered molecular maser line was quickly detected in a multitude of similar sources.

Any useful theory of the hydrogen maser phenomenon must directly address this striking fact.

In this paper we have attempted to show that, although hydrogen may be common, the physical conditions necessary for creating a high gain HRL line maser are rather special: for every line (or narrow group of lines) only a limited range of density is able to producing the high negative values of the local absorption coefficients required. Furthermore the region with this special density must be adequately extended, and homogeneous enough in its radial velocity, to create an optical depth  $< -1$ . The velocity



dispersion parameter is an especially important one. One of the advantages of molecular masers is that they are located in relatively cold, neutral gas clouds and are produced by relatively heavy particles, so the width of the local thermal velocity profile is, in general, only  $\sim 1 \text{ km s}^{-1}$ . Together with the high density of these cold clouds, such a small velocity dispersion can produce over even a short distance a high negative optical depth at the line center, and thus very strong masing. A HRL maser, on the other hand, is generated in a hot ionized gas and is radiated by the lightest particle, whose thermal velocity dispersion is therefore very high,  $\sim 20 \text{ km s}^{-1}$ . As a result the local absorption coefficient is relatively low, regardless of the degree of inversion, and so long distances are required to create  $\tau < -1$ . But longer distances bring an additional velocity dispersion to the picture due to their large scale motions — expansion, contraction, and the like, which broaden the frequency profile of the amplified radiation even more, thus hindering strong masing.

In such situations *chance* may become a decisive factor for creating an *observable* maser. In the case of MWC349, there are at least two lucky coincidences: (1) a very high UV- luminous star, perhaps in a particular outflow phase of its life, surrounded by a dense, massive neutral disk, resulting in an unusually dense, extended HII region on the disk’s surface; and (2), a fortuitous projection of the disk to our line-of-sight as edge-on. A Keplerian velocity field seen edge-on is a better “organizer” of the atoms’ radial velocities than an outflow — that is why we observe stronger mm and submm masers from the disk of MWC349 than from its outflow (cf. Paper 3).

Whatever the particulars of HRL line masers and lasers, nature is fabulously inventive. Conditions favorable to the creation of rather strong hydrogen masers and lasers, or even abnormally strong absorbers (dasars), might occur in several classes of astrophysical objects, both galactic and extra-galactic. The strong hydrogen maser in MWC349 was discovered accidentally, during a routine search for more recombination lines in this well-known emission line star, at a time when the paradigm of “decrease of stimulated emission effects toward higher frequencies” was strongly held. Now, thanks to the example of MWC349 coupled with a thorough analysis of high density hydrogen level populations, we can be much more optimistic about finding this intrinsically interesting and informative phenomenon elsewhere in the Universe.

The authors are grateful to D.G. Hummer and P.J. Storey for the possibility of using their machine-readable hydrogen population calculation files prior to their publication. V.P. thanks the partial support of this research by the Tomalla Foundation Fellowship and the International Center for Fundamental Physics in Moscow for its help in obtaining this Fellowship. VSS and VOP thank the Smithsonian Institution, National Air and Space Museum for a senior fellowship and visiting fellowship, respectively, to work in the Laboratory for Astrophysics on this program and related observations. Together with HAS they acknowledge financial support from the Institution’s Scholarly Studies Program. HAS also acknowledges partial support from NASA grant NAGW-1711.

## REFERENCES

- Baker, J.G., and Menzel, D.H. 1938, *Ap. J.* , **88**, 52.
- Brockleherst, M., and Seaton, M.J. 1972, *M.N.R.A.S.*, **157**, 179.
- Cillíe, G.G. 1936, *M.N.R.A.S.*, **96**, 771.
- Elitzur, M. 1992, *Astronomical Masers*, Boston: Kluwer.
- Gee, C. S., Percival, I. C., Lodge, J. G., and Richards, D. 1976, *M.N.R.A.S.*, **175**, 209.
- Goldberg, L. 1966, *Ap. J.* , **144**, 1225.
- Gordon, M.A. 1992, *Ap. J.* , **387**, 701.
- Gordon, M.A. 1994, *Ap. J.* , **421**, 314.
- Hummer, D.G., and Storey, P.J. 1992, *M.N.R.A.S.*, **254**, 277.
- Krolik, J.H. and McKee, C.F. 1978, *Ap. J. Suppl.*, **37**, 459.
- Kronberg, P.P., Biermann, P., and Schwab, F.R. 1985, *Ap. J.* , **291**, 693.
- Kurtz, S., Churchwell, E., and Wood, D.O.S. 1993, *Ap. J. Suppl.*, **91**, 659.
- Martín-Pintado, J., Bachiller, R., Thum, C., and Walmsley, C.M. 1989a, *Astr. Ap.*, **215**, L13.
- Martín-Pintado, J., Thum, C., Bachiller, R. 1989b, *Astr. Ap.*, **229**, L9.
- Menzel, D.H. 1937, *Ap. J.* , **85**, 330.
- Osterbrock, D.E. 1989, *Astrophysics of Gaseous Nebulae and Active Galactic Nuclei*, Mill Valley, CA: University Sci.Books.
- Planesas, P., Martín-Pintado, J., and Serabyn, E. 1992, *Ap. J. (Letters)*, **386**, L23.
- Ponomarev, V.O. 1994, *Pis'ma v Astron. Zh.* , **20**, 184.
- Ponomarev, V.O., Smirnov, G.T., Strel'nitski, V.S., Chugai, N.N. 1989, *Astron. Tsirk.* , **1540**, 5.
- Ponomarev, V.O., Strel'nitski, V.S., Chugai, N.N. 1991, *Astron. Tsirk.* , **1545**, 37.
- Ponomarev, V.O., Smith, H.A., and Strel'nitski, V.S. 1994, *Ap. J.* , **424**, 976.
- Reid, M.J. and Moran, J.M. 1981, *Ann. Rev. Astr. Ap.*, **19**, 231.
- Rosseland, S. 1926, *Ap. J.* , **63**, 218.
- Scoville, N.Z., and Norman, C.A. 1988, *Ap. J.* , **332**, 163.
- Scoville, N.Z., and Norman, C.A. 1995, in preparation.
- Shaver, P.A., Churchwell, E., and Rots, A.H. 1977, *Astr. Ap.*, **55**, 435.
- Seaton, M.J. 1959, *M.N.R.A.S.*, **119**, 90.
- Slettebak, A., Collins II, G.W., and Truax, R., 1992, *Ap. J. Suppl.*, **81**, 335.
- Smith, H.A., Larson, H.P., and Fink, U. 1979, *Ap. J.* , **233**, 132.
- Smith, H.A., Strel'nitski, V.S., Thum, C., and Martín-Pintado, J. 1995, in preparation.
- Sobolev, A.M., Strel'nitski, V.S., and Chugai, N.N. 1985, *Astrofísica* , **22**, 613.
- Storey, P.J., and Hummer, D.G. 1995, *M.N.R.A.S.*, **272**, 41.
- Strel'nitski, V.S. 1974, *Soviet Physics Uspekhi* , **17**, 507.
- Strel'nitski, V.S. 1983, *Nauchnye Informatsii Astron. Council USSR Ac. Sci.* , **52**, 75. (Spanish translation: *Ciencia*, **43**, 185.)
- Strel'nitski, V.S. 1984, *M.N.R.A.S.*, **207**, 339.
- Strel'nitski, V.S. 1993, In: "Astrophysical Masers," Proceedings of a Conference Held in Arlington, Virginia, USA 9-11 March 1992, ed. A.W. Clegg and G.E. Nedoluha; Springer-Ferlag, Berlin etc., 1993, p.15.
- Strel'nitski, V.S., Smith, H.A., Haas, M.R., Colgan, S.W.J., Erickson, E.F., Geis, N., Hollenbach, D.J., and Townes, C.H. 1995a, In: Proceedings of the Airborne Astronomy Symposium on the Galactic Ecosystem: From Gas to Stars to Dust, ed. M.R. Haas, J.A. Davidson, and E.F. Erickson; San-Francisco: ASP; p.271.
- Strel'nitski, V.S., Smith, H.A., and Ponomarev, V.O. 1995b, *Ap. J.* , submitted ("Paper 3").
- Thum, C., Martín-Pintado, J., and Bachiller, R. 1992, *Astr. Ap.*, **256**, 507.
- Thum, C., Matthews, H.E., Martín-Pintado, J., Serabyn, E., Planesas, P., and Bachiller, R. 1994a, *Astr. Ap.*, **283**, 582.
- Thum, C., Matthews, H.E., Harris, A.I., Tacconi, L.J., Shuster, K.F., and Martín-Pintado, J. 1994b, *Astr. Ap.*, **288**, L25.
- Thum, C., Strel'nitski, V.S., Martín-Pintado, J., Matthews, H.E., and Smith, H.A. 1995, *Astr. Ap.*, submitted.
- Walmsley, C.M. 1990, *Astr. Ap. Suppl. Ser.*, **82**, 201.
- Wood, D.O.S., and Churchwell, E. 1989, *Ap. J. Suppl.*, **69**, 831.

## FIGURE CAPTIONS

Fig. 1. To the classification of non-LTE states of a quantum transition.

Fig. 2. *Solid lines*:  $b_n(n)$  at  $T_e = 10^4$  K and at different electron number densities  $N_e$  ( $\text{cm}^{-3}$ ), indicated near the curves. Numerical data from Storey and Hummer (1995). *Broken line*:  $b_n(n)$  at  $N_e = 0$  (“radiative limit”), calculated with the program of one of us (V.P.) mentioned in text.

Fig. 3. To the explanation of the overcooling mechanism:  $b_{nl}(l)$  for  $n = 30 - 45$ , at  $T_e = 10^4$  K and  $N_e = 10^3 \text{ cm}^{-3}$ . Note the rearrangement of the  $b_{nl}$  factors in favor of the high- $l$  sublevels with the decrease of  $n$ , due to the increasing unblurring of the  $l$ -structure. Numerical data from Storey and Hummer (1995).

Fig. 4. *a* —  $\beta_{n,n+1}(n)$  at  $T_e = 10^4$  K and at  $N_e = 10^3 - 10^7 \text{ cm}^{-3}$  (numbers near the curves). *b* — The same for  $N_e = 10^8 - 10^{12} \text{ cm}^{-3}$ . Numerical data from Storey and Hummer (1995).

Fig. 5.  $\beta_{n,n+1}(N_e)$  at  $T_e = 10^4$  K for different  $n\alpha$  lines ( $n$  is indicated near the curves). Numerical data from Storey and Hummer (1995). The bars, in the lower part of the figure, show the location and the width (FWHM) of the  $k_l(N_e)$  and  $k_{net}(N_e)$  profiles for the  $36\alpha$  line, according to our calculations (compare with Fig. 6b).

Fig. 6. *a-i* —  $k_{net}(N_e)$  for some  $\alpha$ -lines at  $T_e = 10^4$  K. *j* —  $k_{net}(N_e)$  at  $T_e = 10^4$  K for some  $\beta$ -lines.

Fig. 7. *Solide lines*:  $\log|k_{net}|(\log N_e)$  for higher  $n$   $\alpha$ -lines ( $n$  is indicated near the curves), for  $T_e = 10^4$  K. *Broken lines* — loci of the maximal  $|k_{net}|$  for individual  $\alpha$ -lines, for  $T_e = 10^4$  and  $5 \cdot 10^3$  K. *Dotted line* — the envelope of the  $|k_{net}|(N_e)$  plots for  $T_e = 5 \cdot 10^3$  K (the plots are not shown).

Fig. 8  $\log|k_{net}|(n)$  for different electron densities, for  $T_e = 10^4$  K (solide lines) and  $5 \cdot 10^3$  K (broken lines).

Fig. 9. *Dots*: Graphical representation of the  $N_e^{max}(n)$  dependence, with the numerical data from Table 1 for  $T_e = 10^4$  K. *Dashed line*: approximation (3.1.2) for  $5 \leq n \leq 40$ .

Fig. 10. The LTE line and continuum absorption coefficients,  $k'_l$  and  $k'_c$ , as functions of  $n$ , for  $T_e = 10^4$  and  $5 \cdot 10^3$  K.

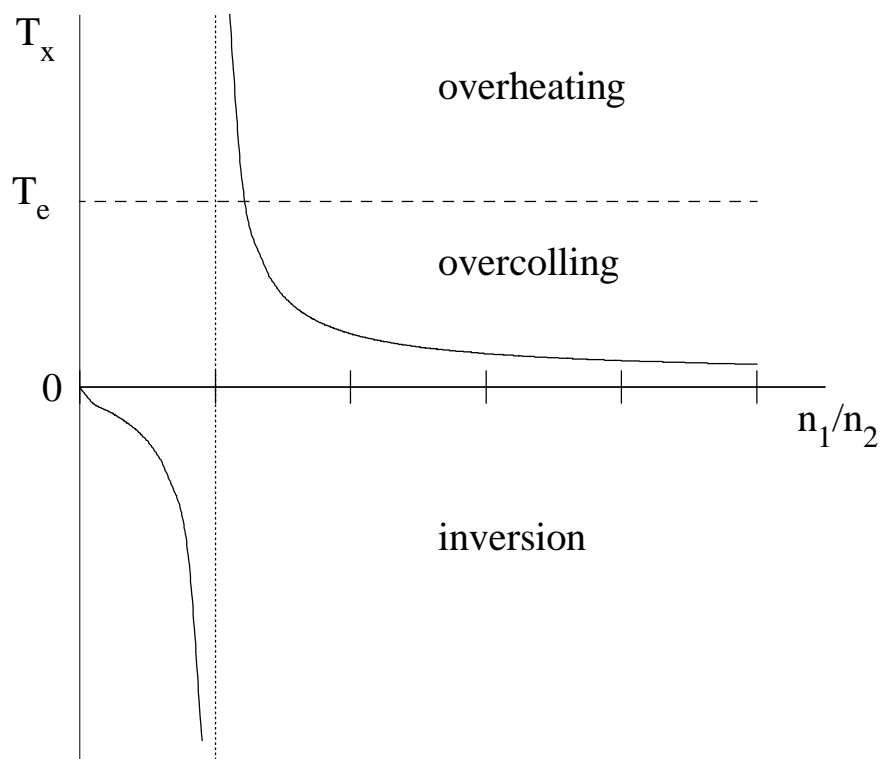
## TABLE CAPTION

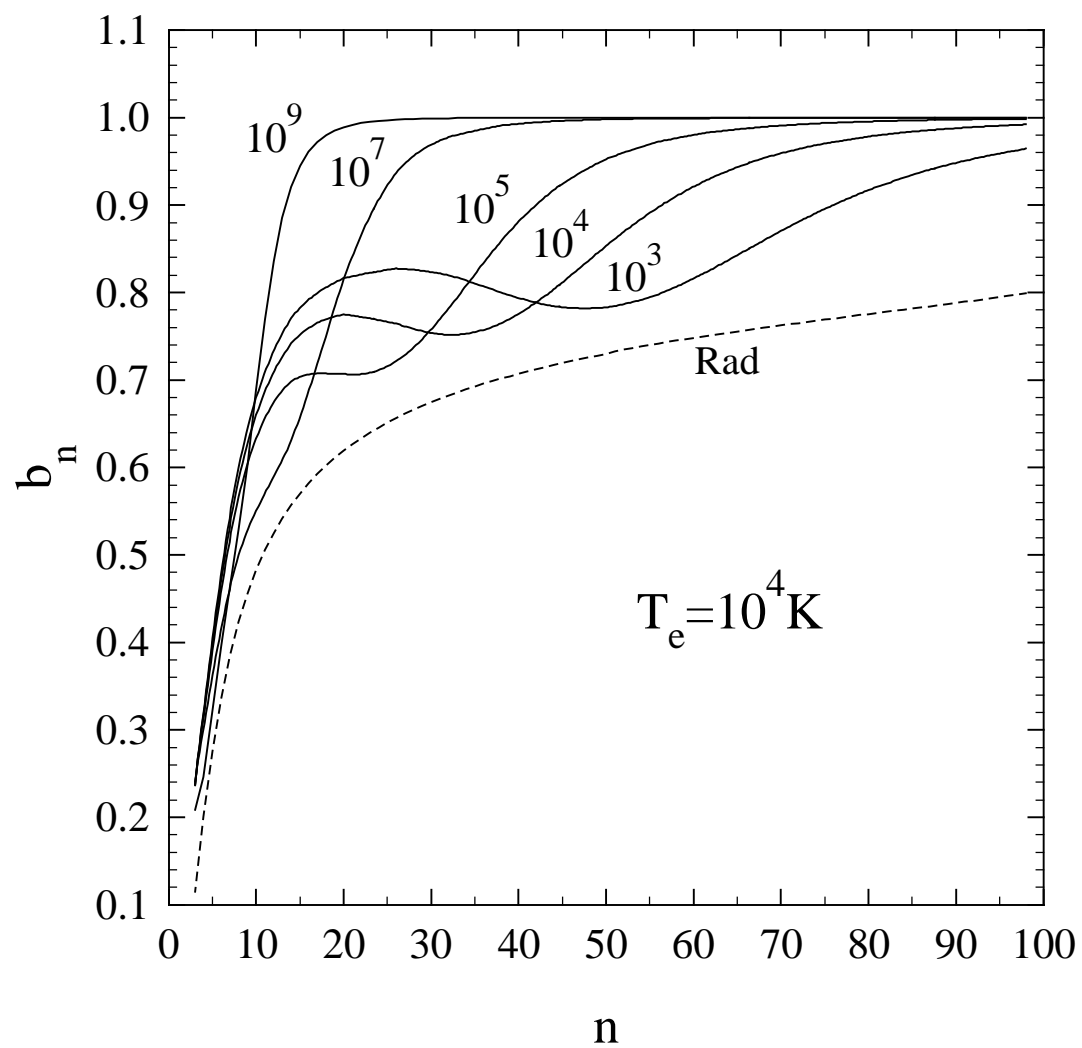
Table 1. Optimum densities of unsaturated maser amplification,  $N_e^{max}$ , and the values of  $k_{net}^{max}$  for hydrogen recombination  $\alpha$ - and  $\beta$ -lines at  $T_e = 10,000$  and  $5,000$  K.

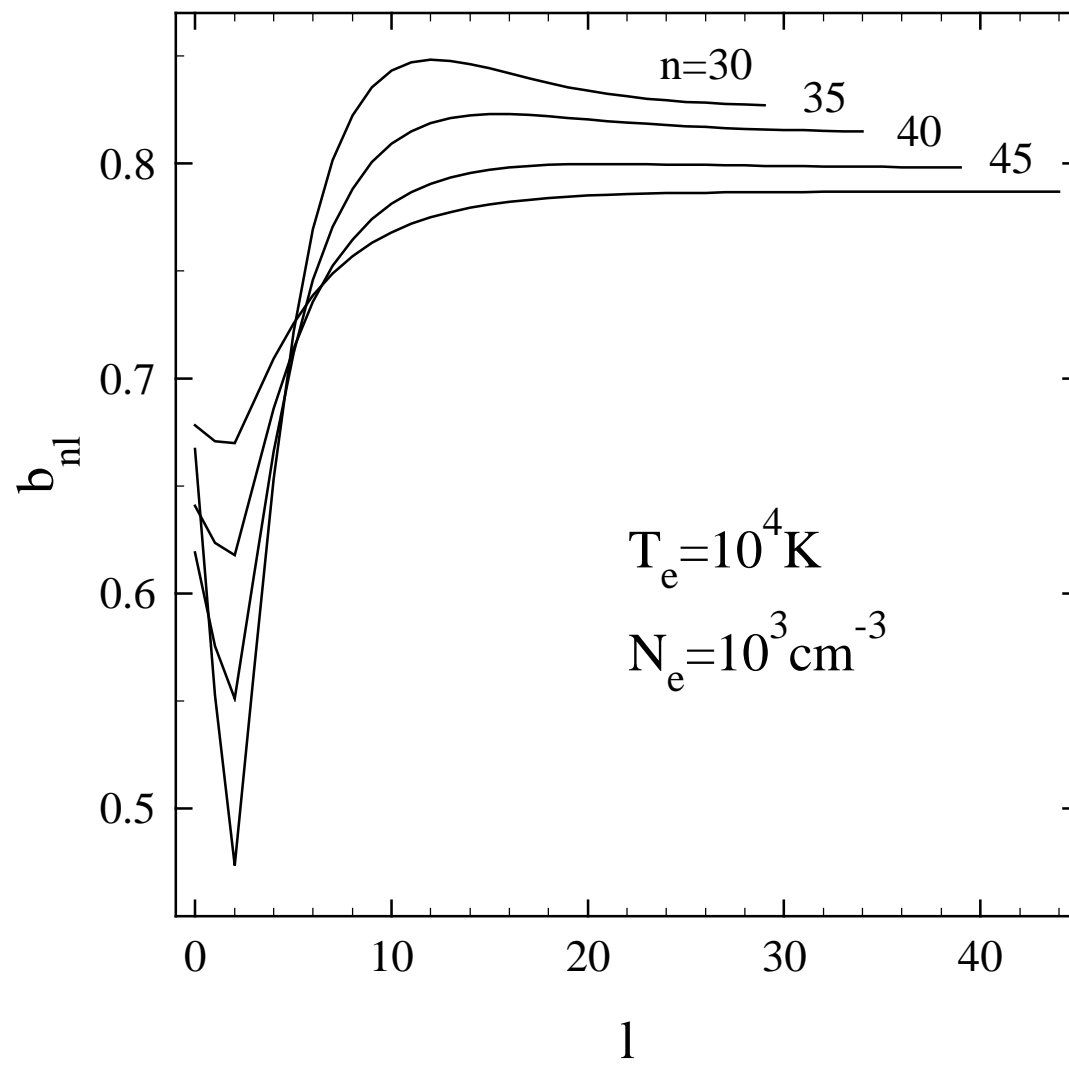
VLADIMIR S. STRELNITSKI: Laboratory for Astrophysics, MRC 321, National Air and Space Museum, Smithsonian Institution, Washington, DC 20560. *e-mail:* vladimir@wright.nasm.edu

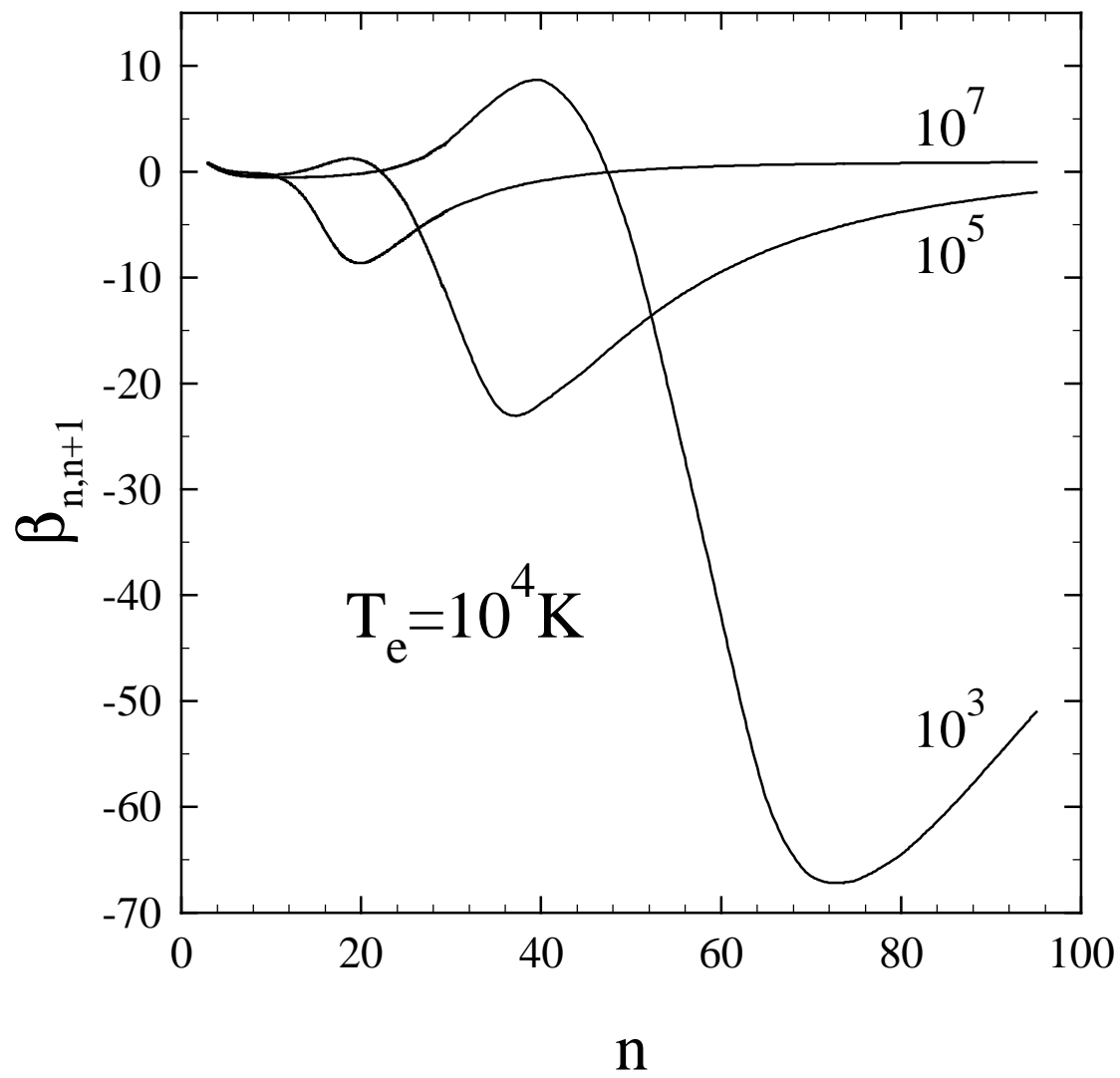
HOWARD A. SMITH: Laboratory for Astrophysics, MRC 321, National Air and Space Museum, Smithsonian Institution, Washington, DC 20560. *e-mail:* howard@wright.nasm.edu

VICTOR O. PONOMAREV: Astro-Space Center of P.N. Lebedev Physical Institute, Leninsky prospect, 53, Moscow 117924. *e-mail:* ponomarev@rasfian.serpukhov.su

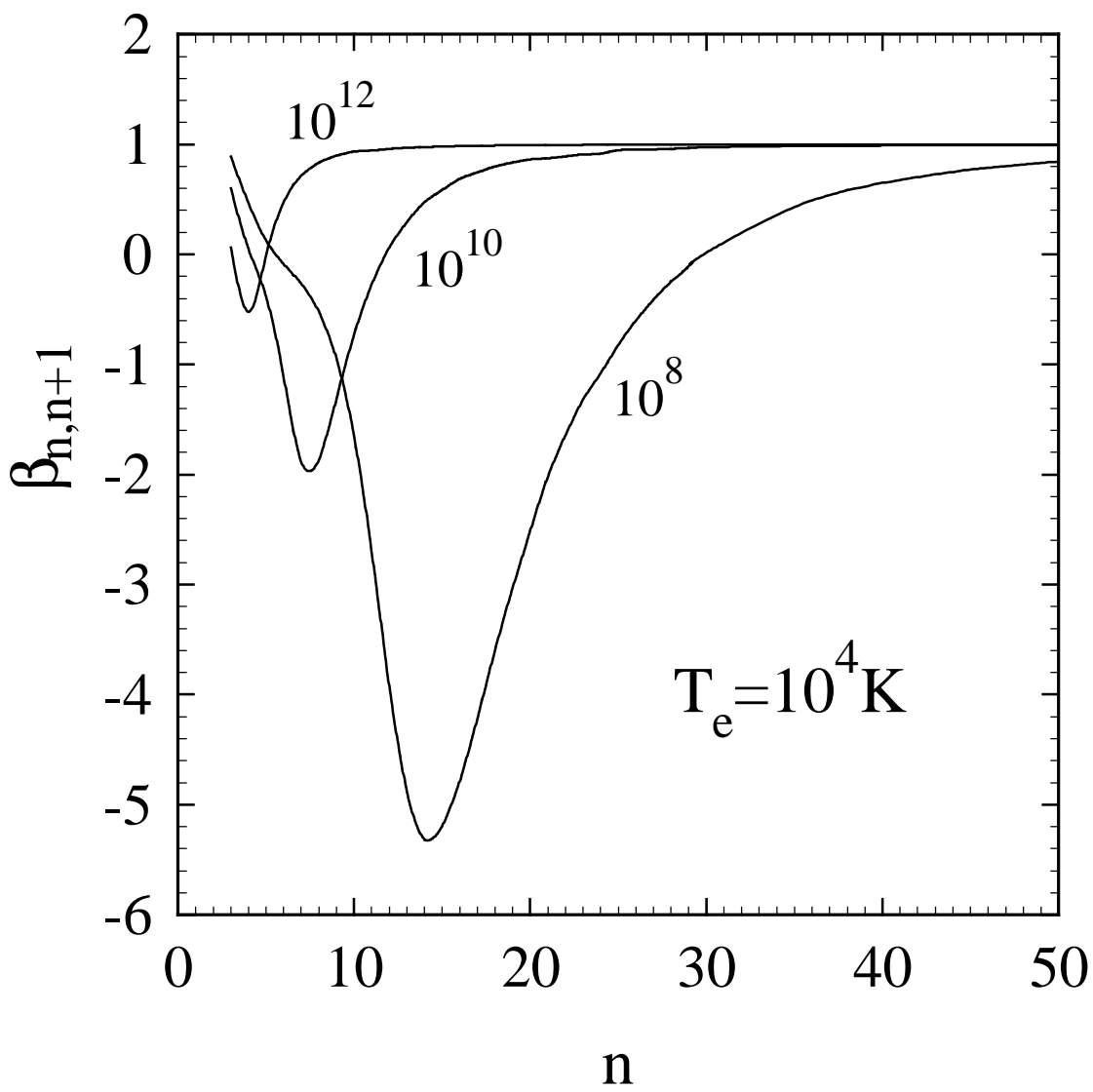


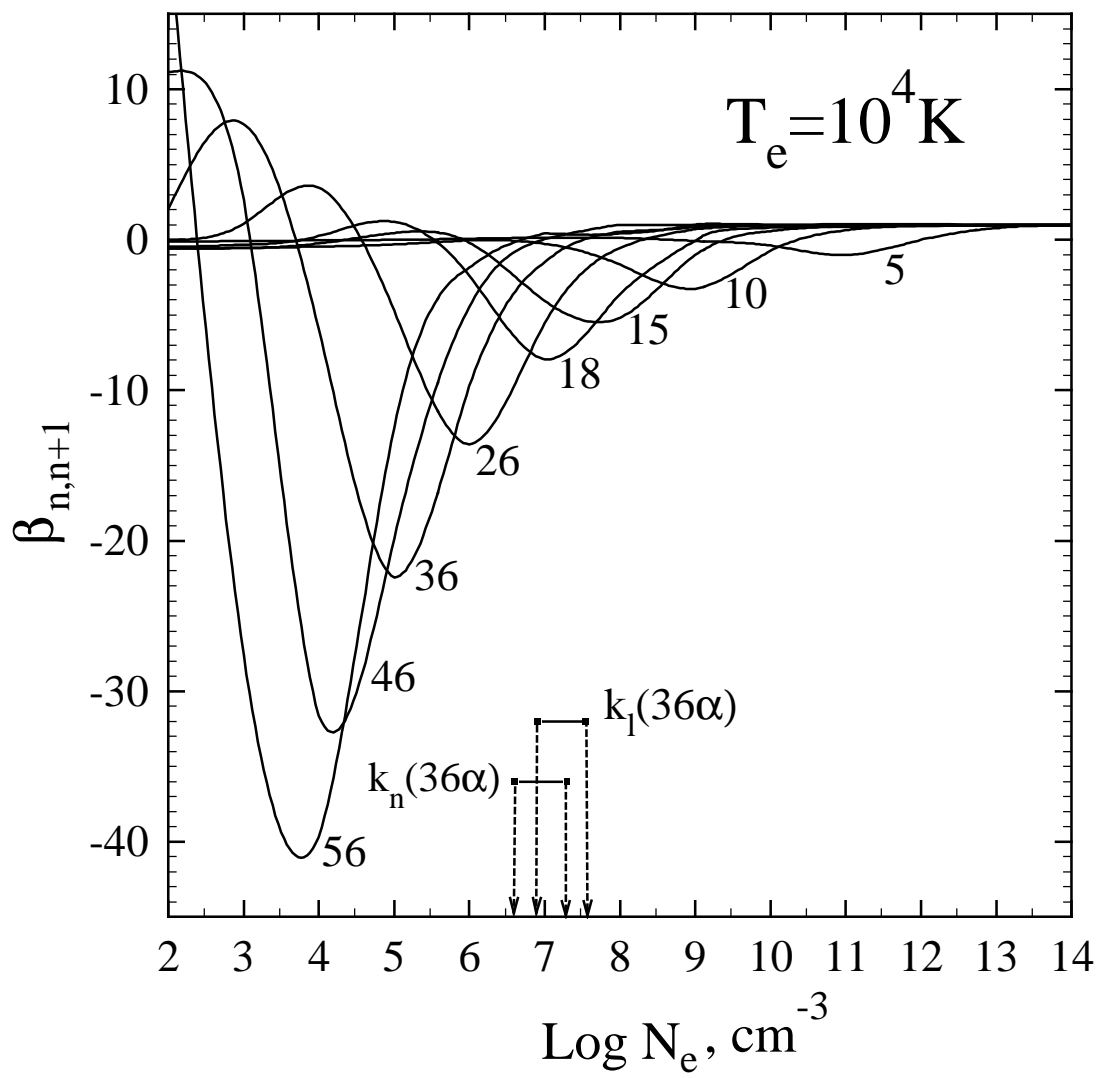


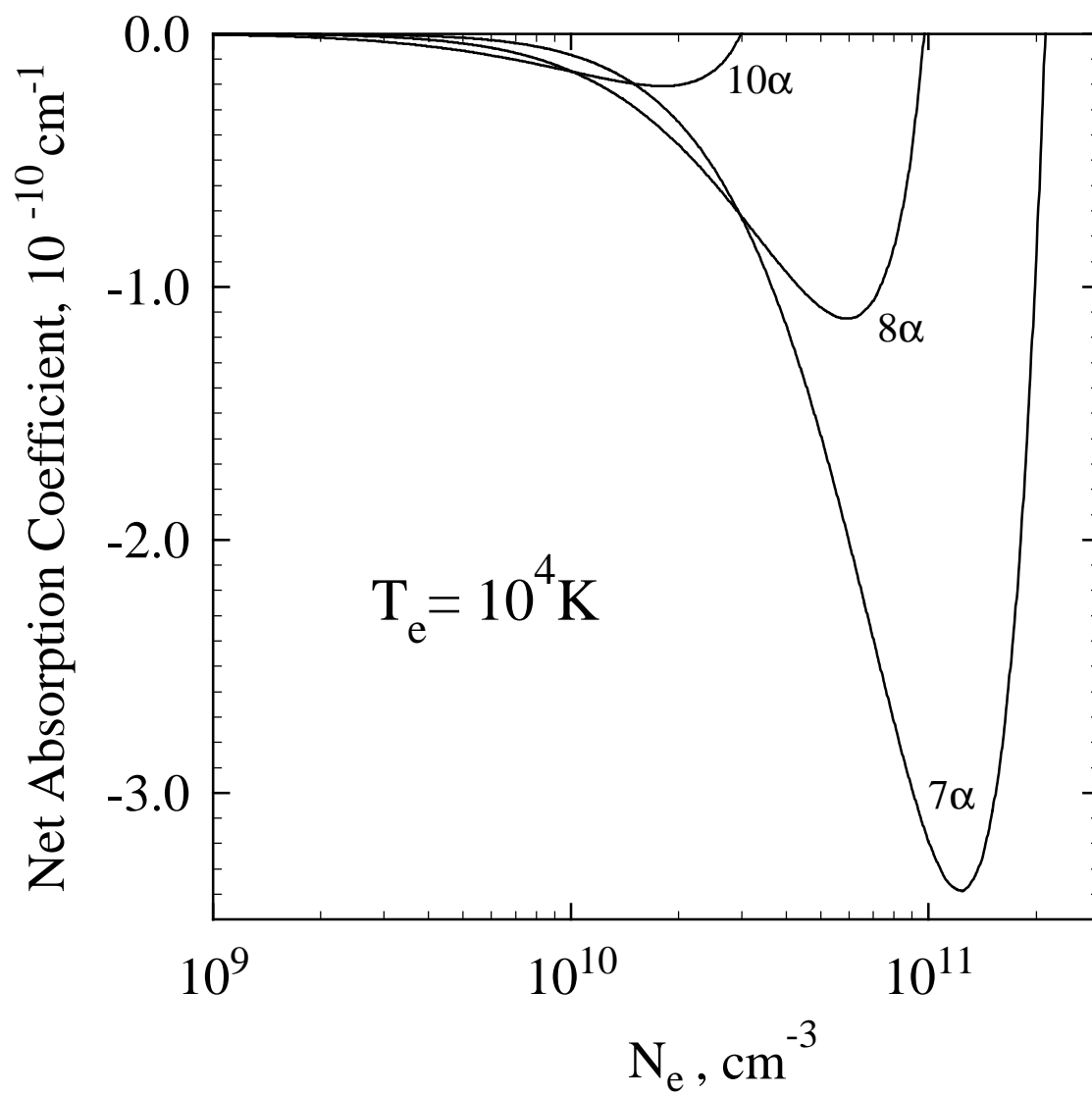


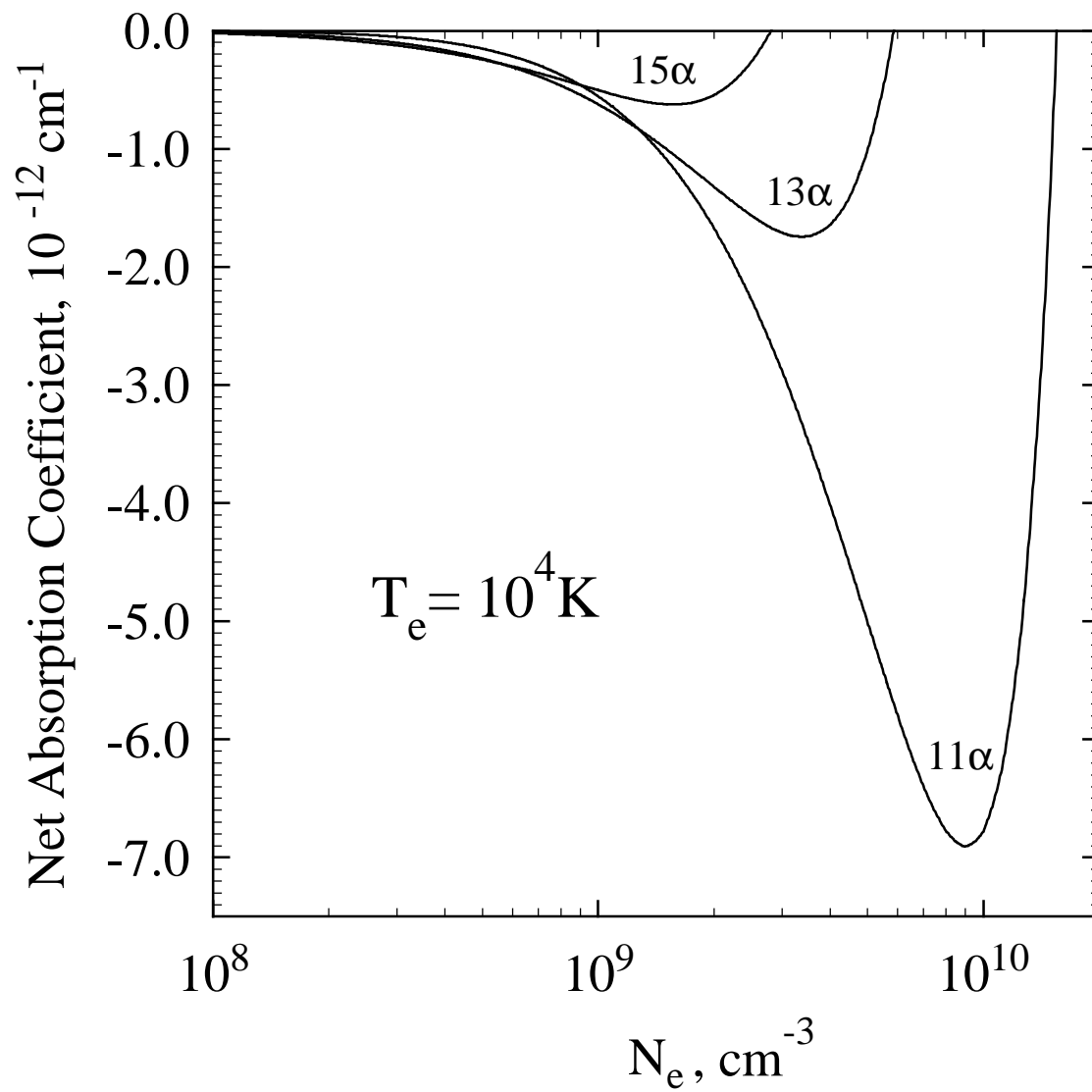


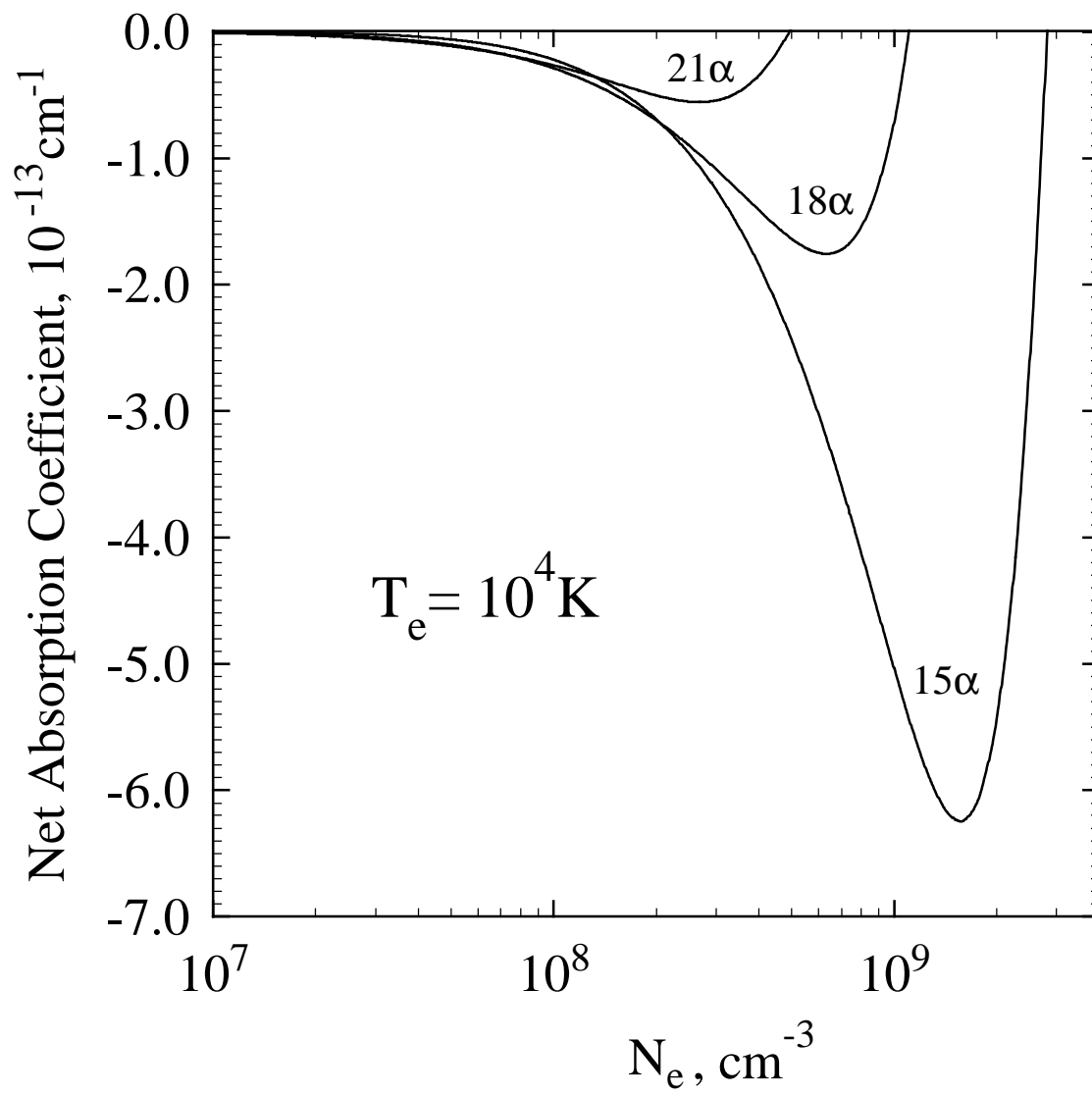


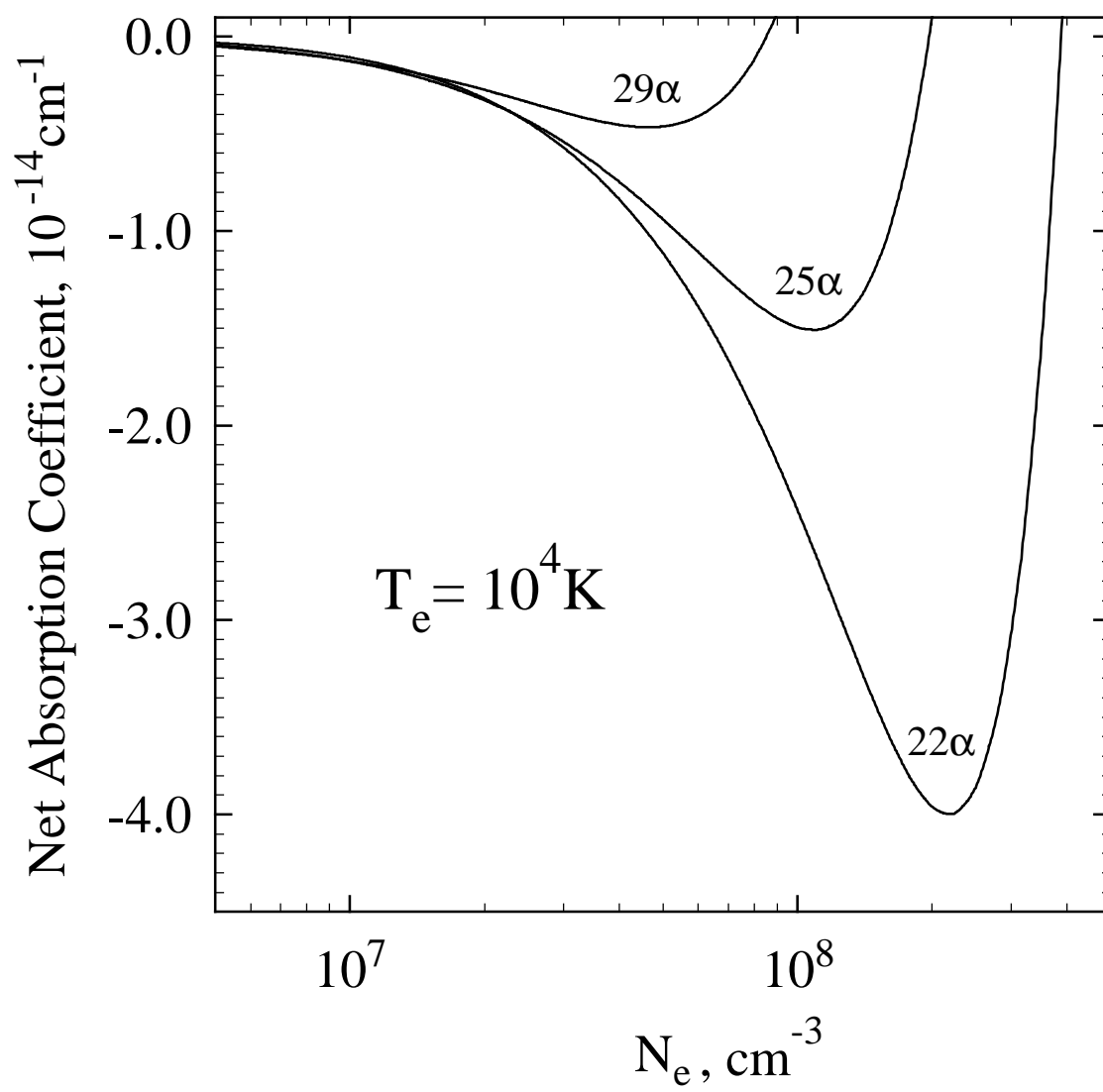


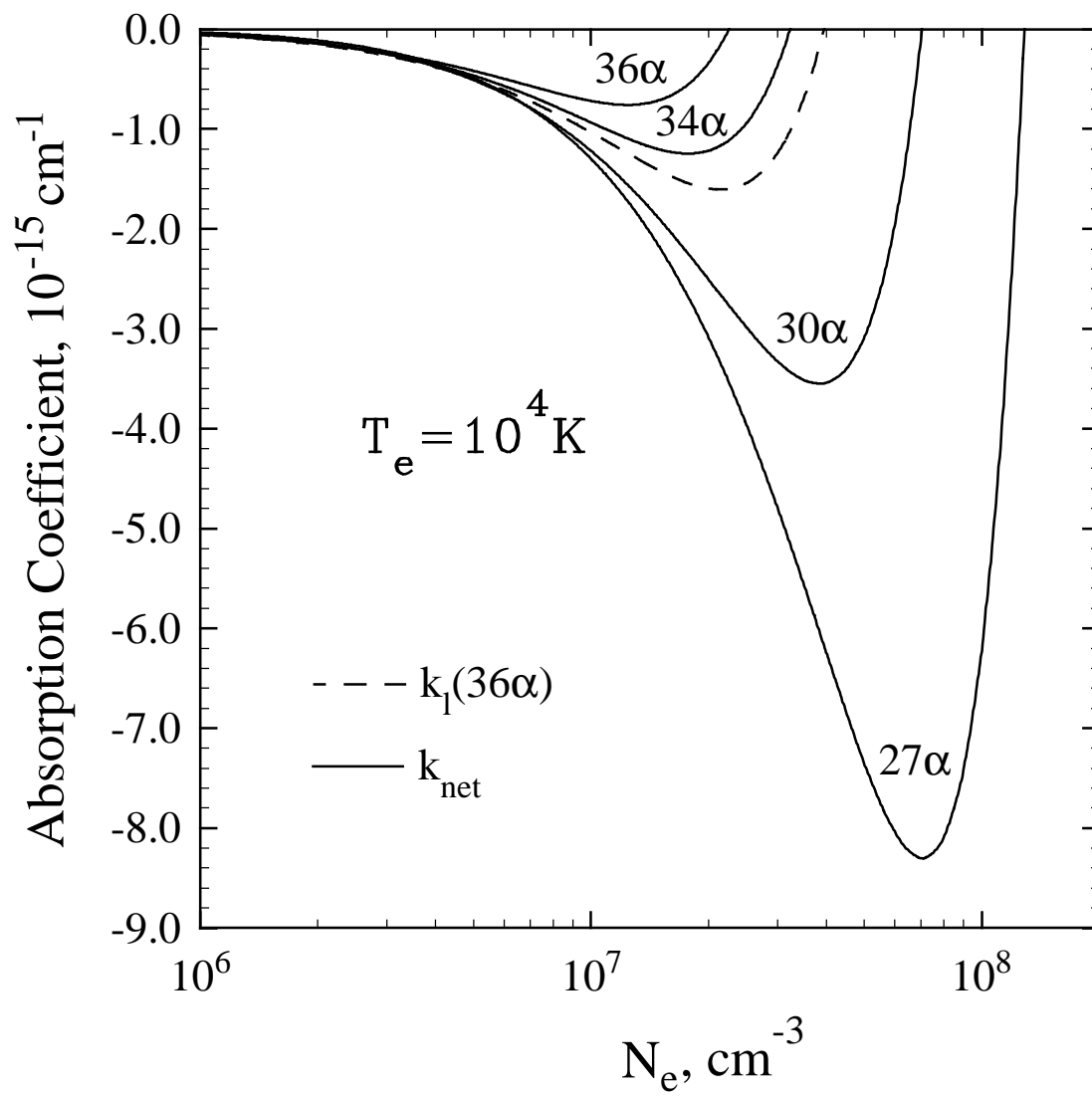


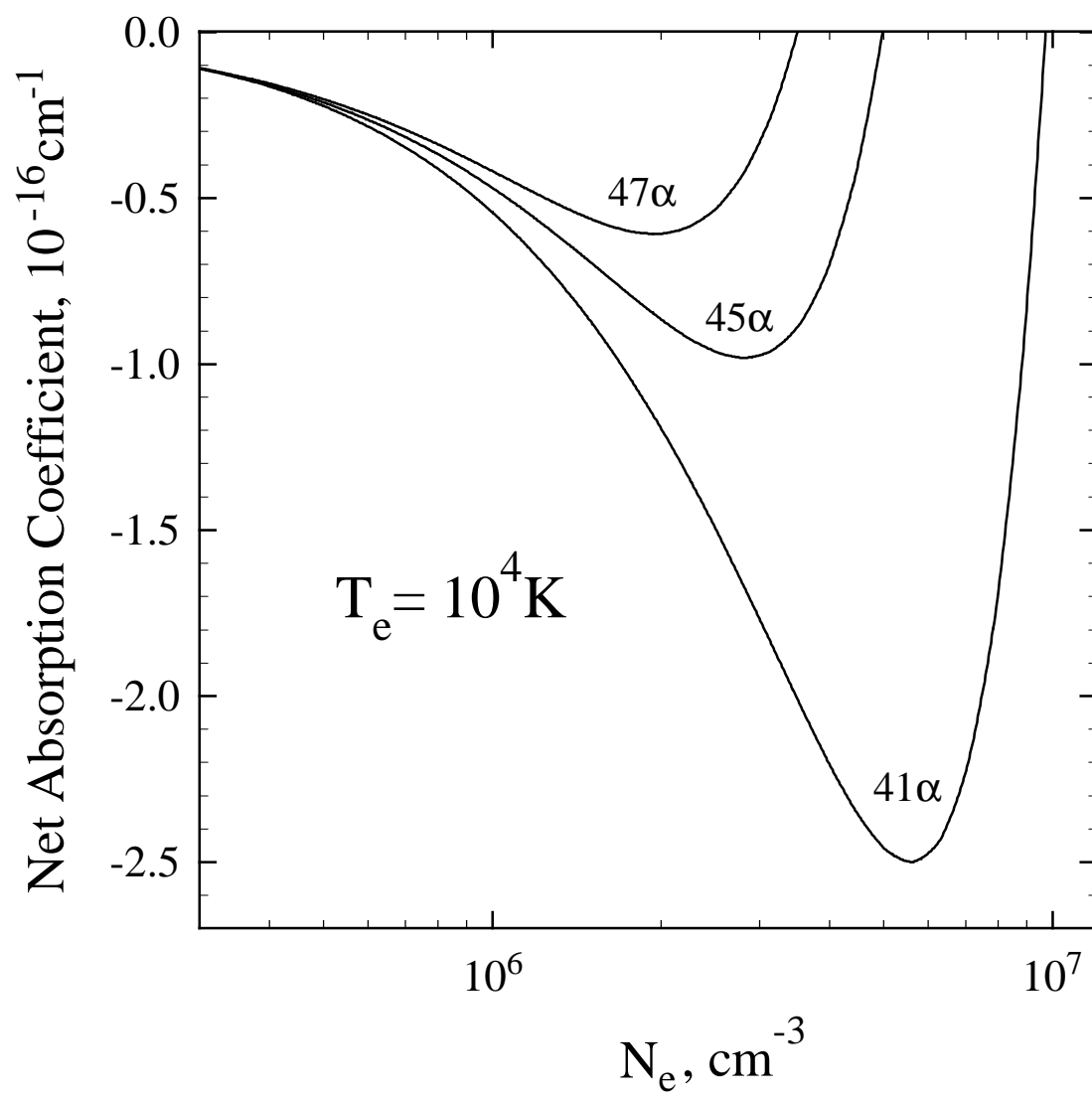




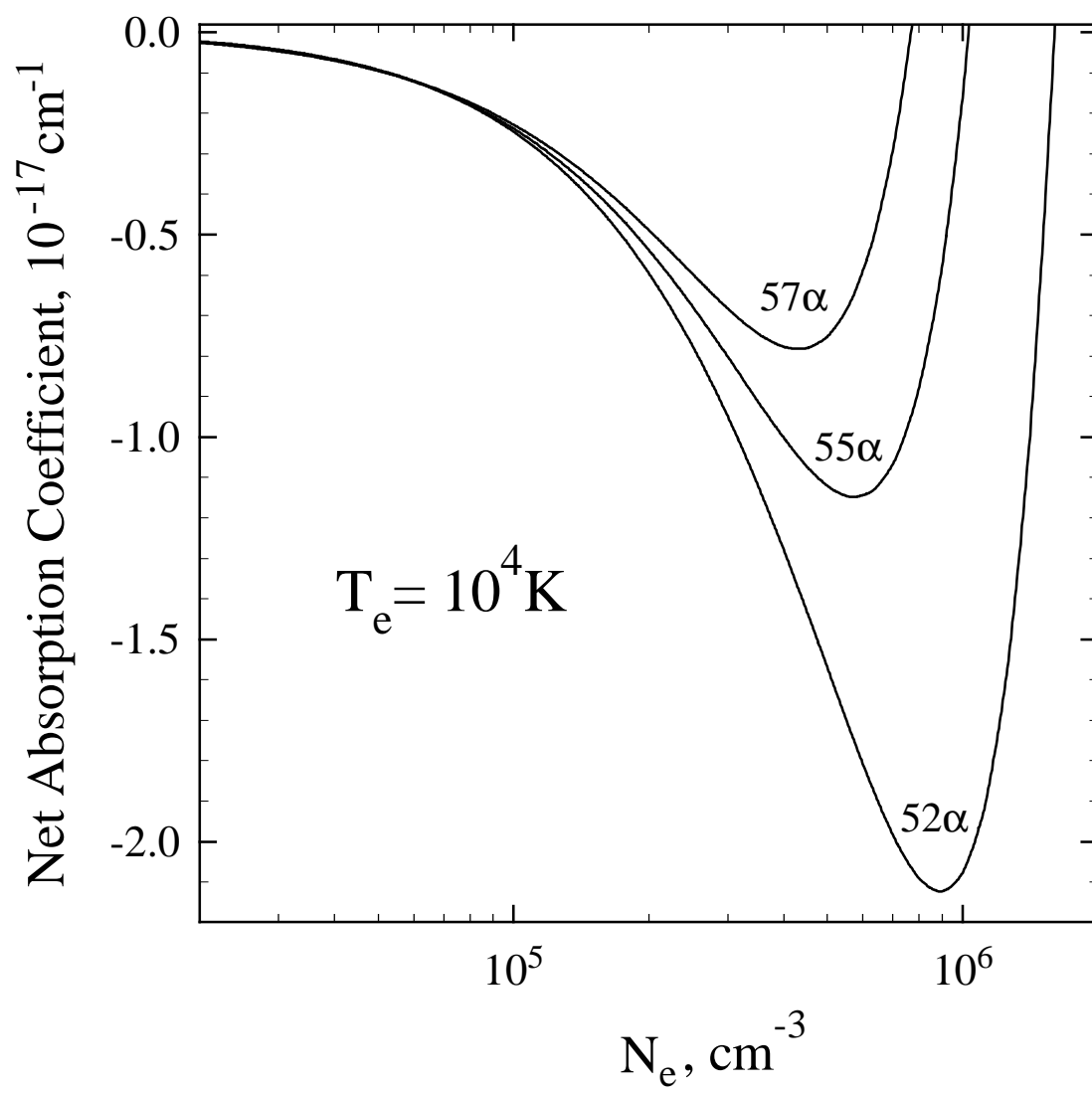


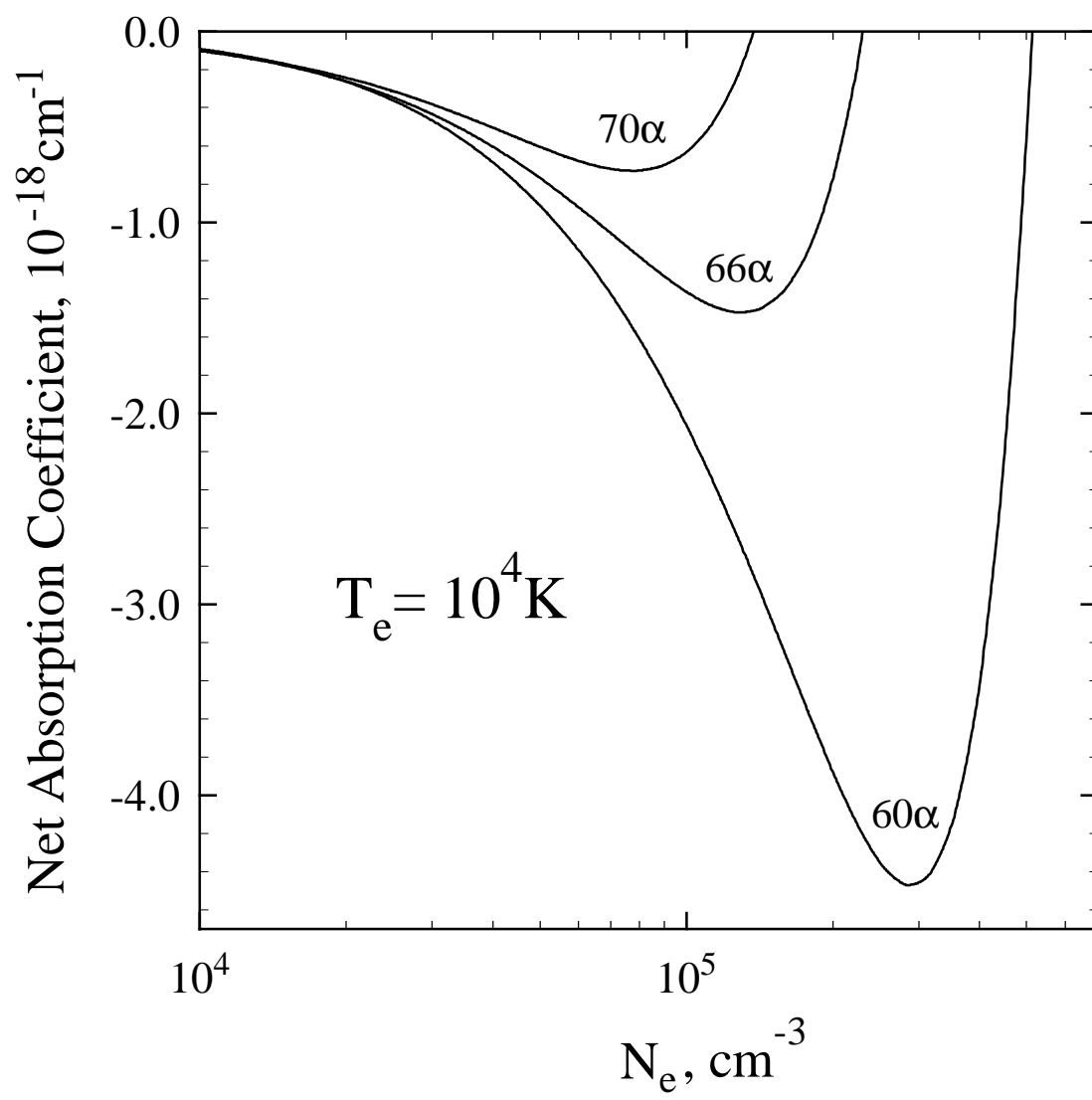


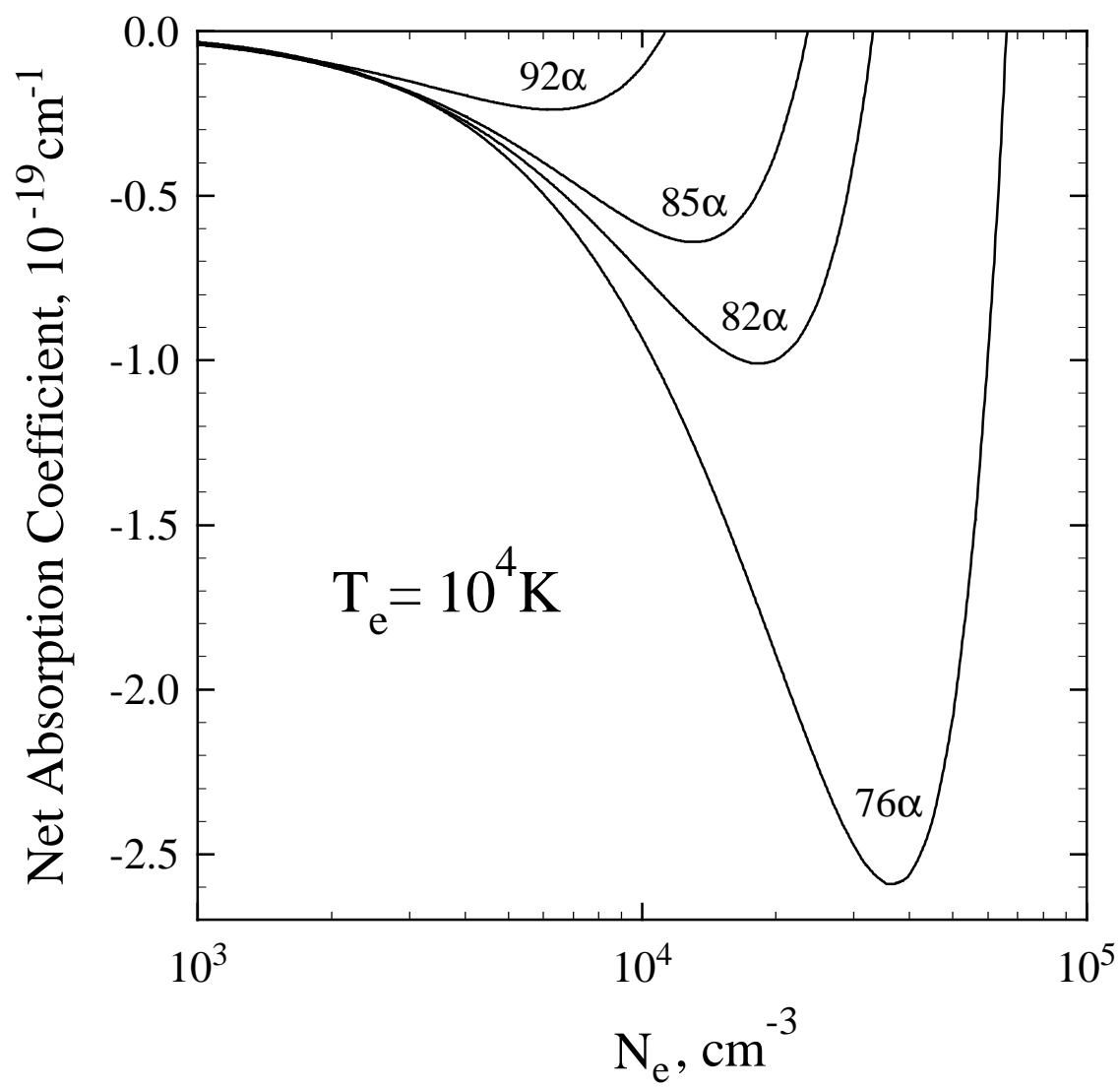


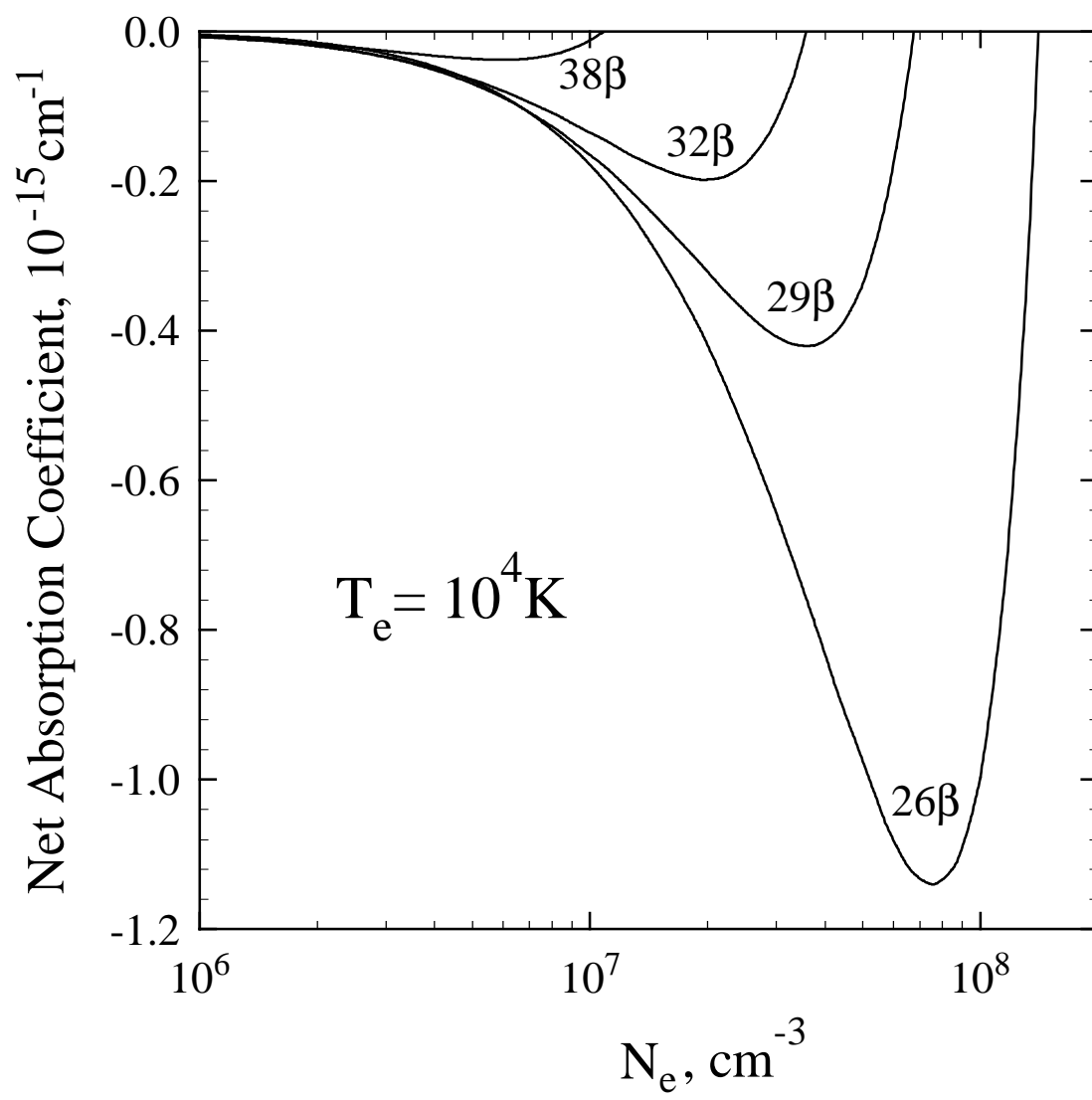


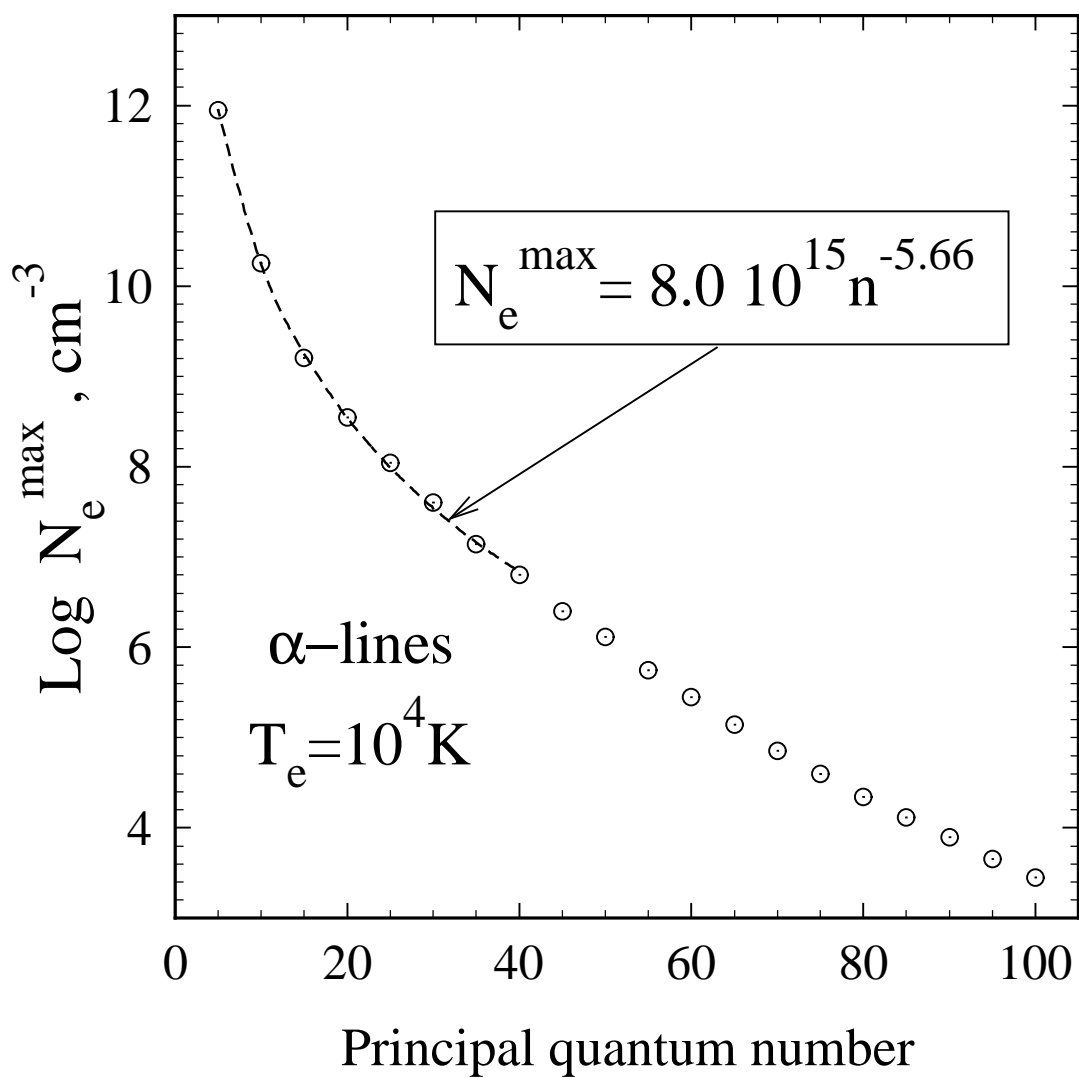


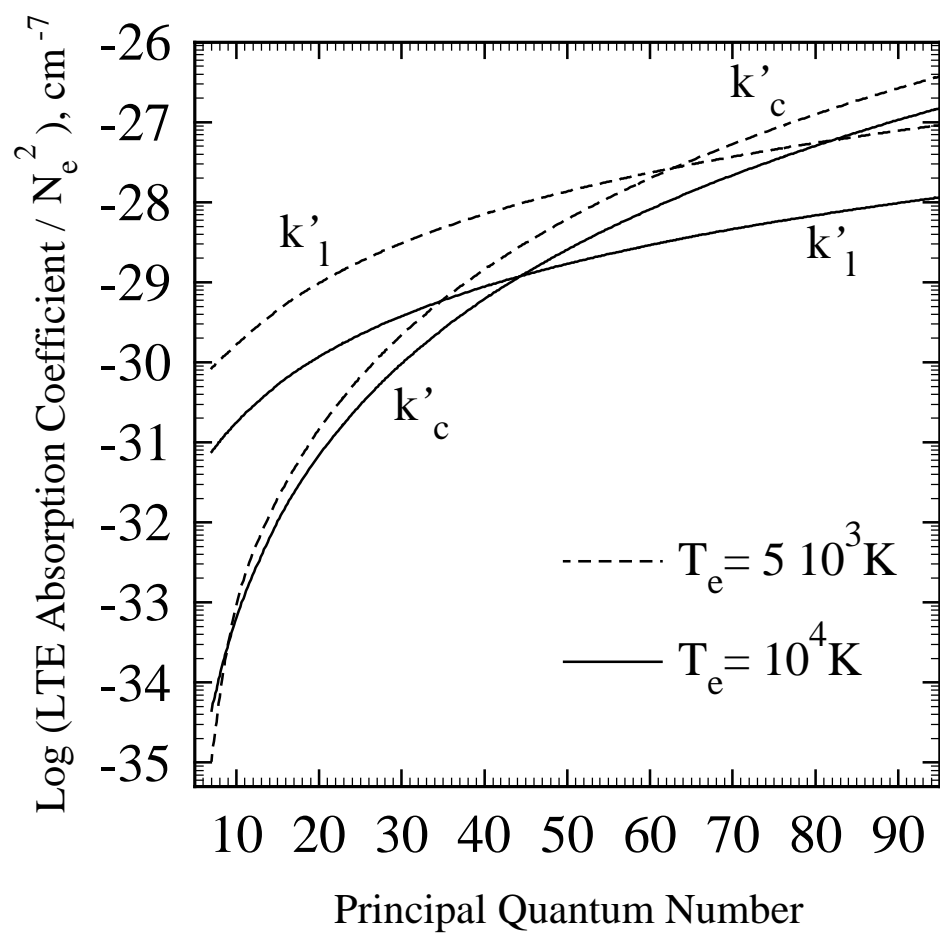


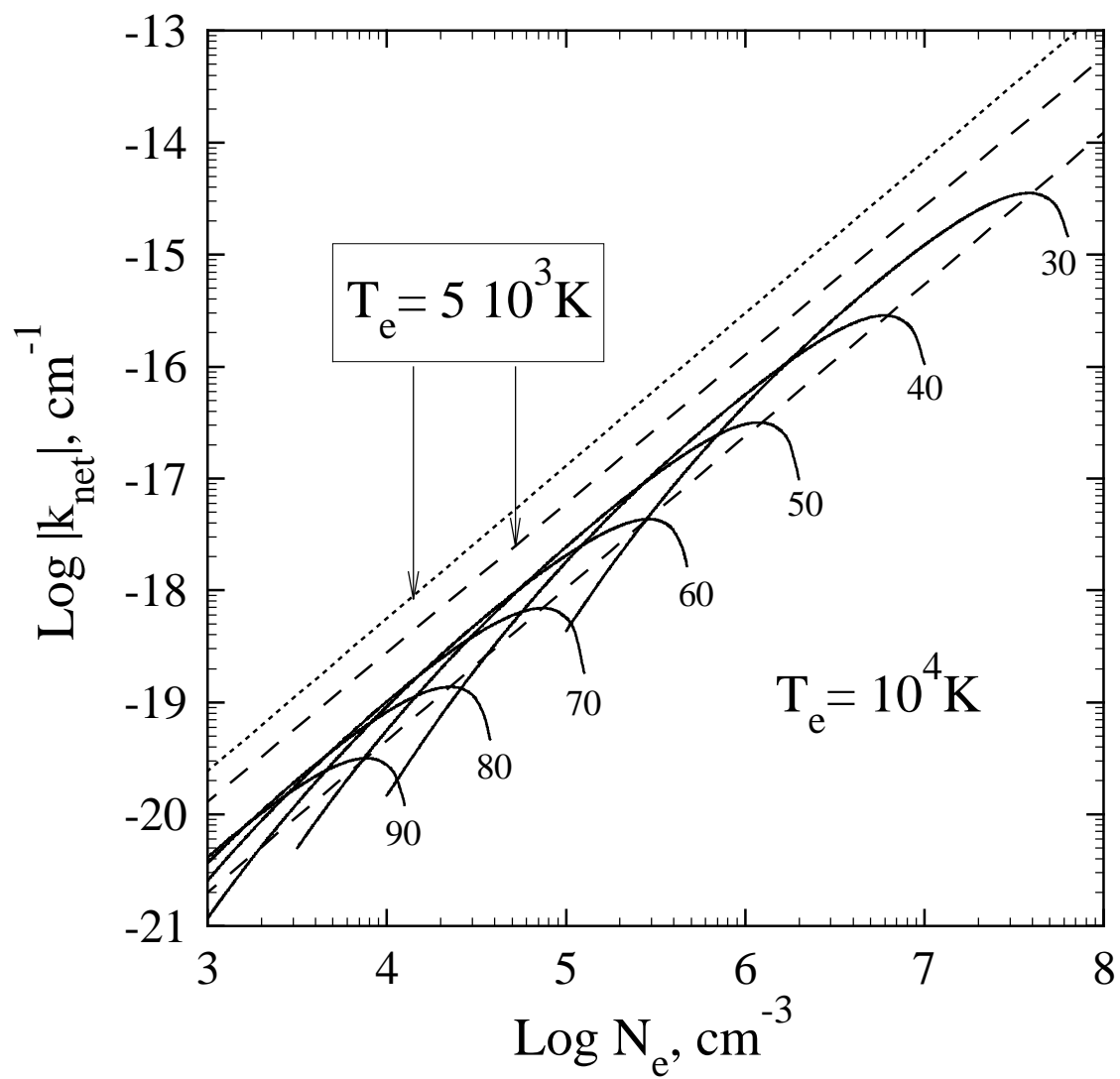


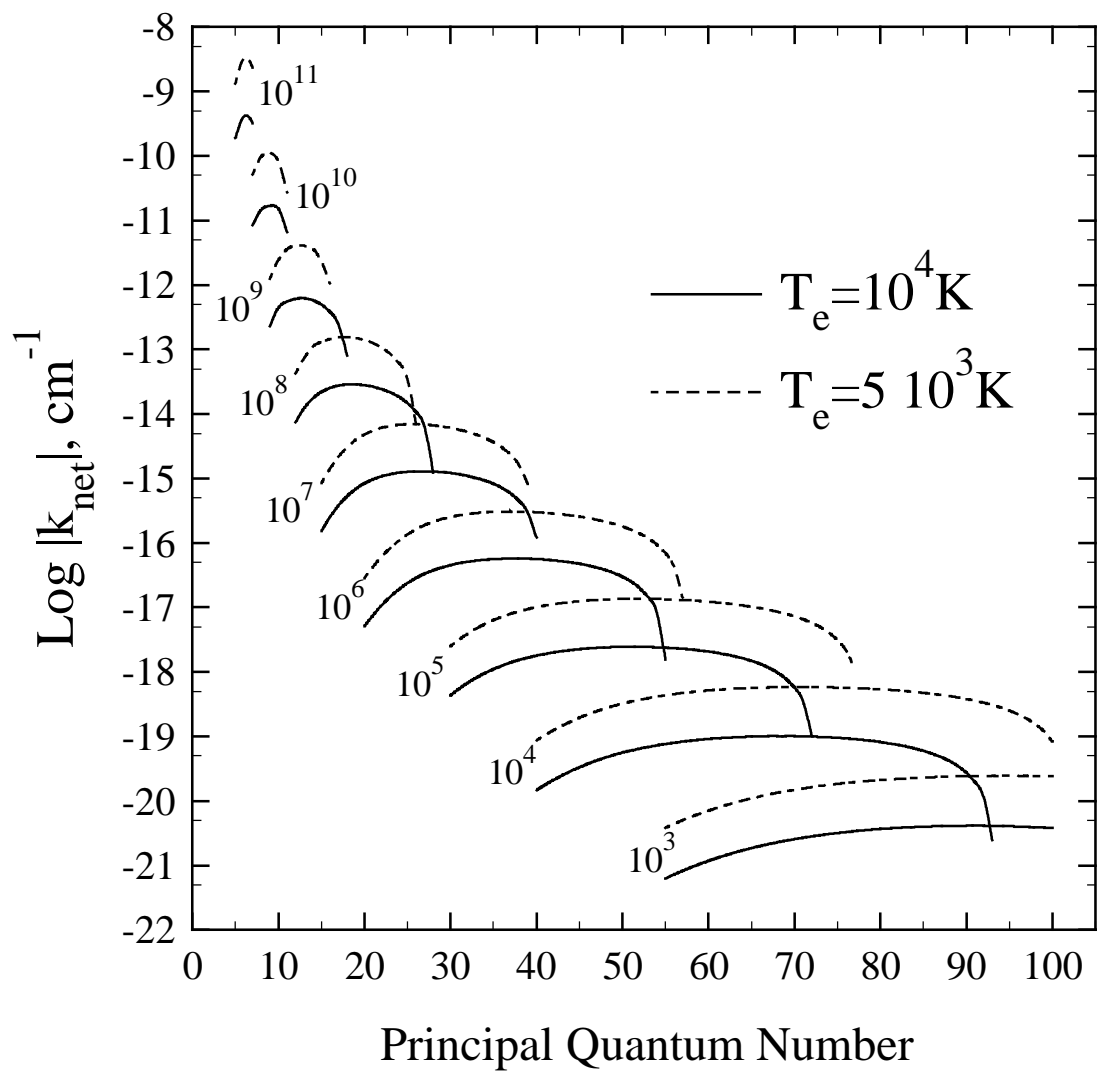














n	$T_e = 5 \cdot 10^3 \text{ K}$				$T_e = 10^4 \text{ K}$			
	$\alpha$ -lines		$\beta$ -lines		$\alpha$ -lines		$\beta$ -lines	
	$k_{net}^{max},$ $\text{cm}^{-1}$	$N_e^{max},$ $\text{cm}^{-3}$	$k_{net}^{max},$ $\text{cm}^{-1}$	$N_e^{max},$ $\text{cm}^{-3}$	$k_{net}^{max},$ $\text{cm}^{-1}$	$N_e^{max},$ $\text{cm}^{-3}$	$k_{net}^{max},$ $\text{cm}^{-1}$	$N_e^{max},$ $\text{cm}^{-3}$
5	$-6.9 \cdot 10^{-8}$	$8.9 \cdot 10^{11}$	$-5.1 \cdot 10^{-9}$	$6.3 \cdot 10^{11}$	$-6.1 \cdot 10^{-9}$	$8.9 \cdot 10^{11}$	$-4.8 \cdot 10^{-10}$	$6.3 \cdot 10^{11}$
10	$-8.8 \cdot 10^{-11}$	$1.3 \cdot 10^{10}$	$-8.8 \cdot 10^{-12}$	$1.0 \cdot 10^{10}$	$-2.1 \cdot 10^{-11}$	$1.8 \cdot 10^{10}$	$-1.8 \cdot 10^{-12}$	$1.3 \cdot 10^{10}$
15	$-2.4 \cdot 10^{-12}$	$1.1 \cdot 10^9$	$-2.6 \cdot 10^{-13}$	$1.0 \cdot 10^9$	$-6.2 \cdot 10^{-13}$	$1.6 \cdot 10^9$	$-7.1 \cdot 10^{-14}$	$1.4 \cdot 10^9$
20	$-2.5 \cdot 10^{-13}$	$2.2 \cdot 10^8$	$-2.9 \cdot 10^{-14}$	$2.0 \cdot 10^8$	$-8.1 \cdot 10^{-14}$	$3.5 \cdot 10^8$	$-9.0 \cdot 10^{-15}$	$3.2 \cdot 10^8$
25	$-4.8 \cdot 10^{-14}$	$7.1 \cdot 10^7$	$-5.6 \cdot 10^{-15}$	$6.3 \cdot 10^7$	$-1.5 \cdot 10^{-14}$	$1.1 \cdot 10^8$	$-1.6 \cdot 10^{-15}$	$8.9 \cdot 10^7$
30	$-1.2 \cdot 10^{-14}$	$2.5 \cdot 10^7$	$-1.4 \cdot 10^{-15}$	$2.2 \cdot 10^7$	$-3.5 \cdot 10^{-15}$	$4.0 \cdot 10^7$	$-3.4 \cdot 10^{-16}$	$2.8 \cdot 10^7$
35	$-3.7 \cdot 10^{-15}$	$1.1 \cdot 10^7$	$-4.1 \cdot 10^{-16}$	$1.0 \cdot 10^7$	$-9.6 \cdot 10^{-16}$	$1.4 \cdot 10^7$	$-8.4 \cdot 10^{-17}$	$1.1 \cdot 10^7$
40	$-1.3 \cdot 10^{-15}$	$5.6 \cdot 10^6$	$-1.4 \cdot 10^{-16}$	$4.5 \cdot 10^6$	$-2.9 \cdot 10^{-16}$	$6.3 \cdot 10^6$	$-2.3 \cdot 10^{-17}$	$4.0 \cdot 10^6$
45	$-4.9 \cdot 10^{-16}$	$2.5 \cdot 10^6$	$-4.9 \cdot 10^{-17}$	$2.0 \cdot 10^6$	$-9.2 \cdot 10^{-17}$	$2.5 \cdot 10^6$	$-6.5 \cdot 10^{-18}$	$1.6 \cdot 10^6$
50	$-2.0 \cdot 10^{-16}$	$1.4 \cdot 10^6$	$-1.8 \cdot 10^{-17}$	$1.0 \cdot 10^6$	$-3.1 \cdot 10^{-17}$	$1.3 \cdot 10^6$	$-2.0 \cdot 10^{-18}$	$7.1 \cdot 10^5$
55	$-8.4 \cdot 10^{-17}$	$7.1 \cdot 10^5$	$-7.2 \cdot 10^{-18}$	$5.0 \cdot 10^5$	$-1.1 \cdot 10^{-17}$	$5.6 \cdot 10^5$	$-6.7 \cdot 10^{-19}$	$3.2 \cdot 10^5$
60	$-3.7 \cdot 10^{-17}$	$4.0 \cdot 10^5$	$-2.9 \cdot 10^{-18}$	$2.5 \cdot 10^5$	$-4.2 \cdot 10^{-18}$	$2.8 \cdot 10^5$	$-2.4 \cdot 10^{-19}$	$1.4 \cdot 10^5$
65	$-1.7 \cdot 10^{-17}$	$2.2 \cdot 10^5$	$-1.2 \cdot 10^{-18}$	$1.4 \cdot 10^5$	$-1.7 \cdot 10^{-18}$	$1.4 \cdot 10^5$	$-8.9 \cdot 10^{-20}$	$7.1 \cdot 10^4$
70	$-7.8 \cdot 10^{-18}$	$1.3 \cdot 10^5$	$-5.4 \cdot 10^{-19}$	$7.9 \cdot 10^4$	$-7.0 \cdot 10^{-19}$	$7.1 \cdot 10^4$	$-3.5 \cdot 10^{-20}$	$3.5 \cdot 10^4$
75	$-3.7 \cdot 10^{-18}$	$7.1 \cdot 10^4$	$-2.4 \cdot 10^{-19}$	$4.5 \cdot 10^4$	$-3.1 \cdot 10^{-19}$	$4.0 \cdot 10^4$	$-1.5 \cdot 10^{-20}$	$2.0 \cdot 10^4$
80	$-1.8 \cdot 10^{-18}$	$4.5 \cdot 10^4$	$-1.1 \cdot 10^{-19}$	$2.5 \cdot 10^4$	$-1.4 \cdot 10^{-19}$	$2.2 \cdot 10^4$	$-6.3 \cdot 10^{-21}$	$1.1 \cdot 10^4$
85	$-9.3 \cdot 10^{-19}$	$2.8 \cdot 10^4$	$-5.5 \cdot 10^{-20}$	$1.4 \cdot 10^4$	$-6.5 \cdot 10^{-20}$	$1.3 \cdot 10^4$	$-2.9 \cdot 10^{-21}$	$6.3 \cdot 10^3$
90	$-4.8 \cdot 10^{-19}$	$1.6 \cdot 10^4$	$-2.7 \cdot 10^{-20}$	$8.9 \cdot 10^3$	$-3.2 \cdot 10^{-20}$	$7.9 \cdot 10^3$	$-1.4 \cdot 10^{-21}$	$3.5 \cdot 10^3$
95	$-2.5 \cdot 10^{-19}$	$1.0 \cdot 10^4$	$-1.4 \cdot 10^{-20}$	$5.6 \cdot 10^3$	$-1.6 \cdot 10^{-20}$	$4.5 \cdot 10^3$	$-6.7 \cdot 10^{-22}$	$2.0 \cdot 10^3$
100	$-1.4 \cdot 10^{-19}$	$6.3 \cdot 10^3$	$-7.3 \cdot 10^{-21}$	$3.2 \cdot 10^3$	$-8.3 \cdot 10^{-21}$	$2.8 \cdot 10^3$	$-3.4 \cdot 10^{-22}$	$1.3 \cdot 10^3$